

**N-loss isotope effects in the Peru oxygen minimum zone studied using
a mesoscale eddy as a natural tracer experiment**

Annie Bourbonnais^{1, a}, Mark A. Altabet¹, Chawalit N. Charoenpong^{2,3}, Jennifer Larkum¹,
Haibei Hu¹, Hermann W. Bange⁴ and Lothar Stramma⁴

¹School for Marine Science and Technology, University of Massachusetts Dartmouth, 706
Rodney French Blvd, New Bedford, MA 02744-1221, USA

²Department of Marine Chemistry and Geochemistry, Woods Hole Oceanographic Institution,
Woods Hole, MA 02543-1050, USA.

³Department of Earth, Atmospheric and Planetary Sciences, Massachusetts Institute of
Technology, Cambridge, MA 02139-4301, USA

⁴GEOMAR Helmholtz Centre for Ocean Research Kiel, Düsternbrooker Weg 20, 24105 Kiel,
Germany

Corresponding author: Annie Bourbonnais, School for Marine Science and Technology,
University of Massachusetts Dartmouth, 706 Rodney French Blvd, New Bedford, MA 02744-
1221, USA

This article has been accepted for publication and undergone full peer review but has not
been through the copyediting, typesetting, pagination and proofreading process which may
lead to differences between this version and the Version of Record. Please cite this article
as doi: 10.1002/2014GB005001

Abstract

Mesoscale eddies in Oxygen Minimum Zones (OMZ's) have been identified as important fixed nitrogen (N) loss hotspots that may significantly impact both the global rate of N-loss as well as the ocean's N isotope budget. They also represent 'natural tracer experiments' with intensified biogeochemical signals that can be exploited to understand the large-scale processes that control N-loss and associated isotope effects (ϵ ; the ‰ deviation from 1 in the ratio of reaction rate constants for the light versus the heavy isotopologues). We observed large ranges in the concentrations and N and O isotopic compositions of nitrate (NO_3^-), nitrite (NO_2^-) and biogenic N_2 associated with an anticyclonic eddy in the Peru OMZ during two cruises in November and December 2012. In the eddy's center where NO_3^- was nearly exhausted, we measured the highest $\delta^{15}\text{N}$ values for both NO_3^- and NO_2^- (up to ~70‰ and 50‰) ever reported for an OMZ. Correspondingly, N deficit and biogenic N_2 -N concentrations were also the highest near the eddy's center (up to ~40 $\mu\text{mol L}^{-1}$). $\delta^{15}\text{N}$ - N_2 also varied with biogenic N_2 production, following kinetic isotopic fractionation during NO_2^- reduction to N_2 and, for the first time, provided an independent assessment of N isotope fractionation during OMZ N-loss. We found apparent variable ϵ for NO_3^- reduction (up to ~30‰ in the presence of NO_2^-). However, the overall ϵ for N-loss was calculated to be only ~13-14‰ (as compared to canonical values of ~20-30‰) assuming a closed system and only slightly higher assuming an open system (16-19‰). Our results were similar whether calculated from the disappearance of DIN ($\text{NO}_3^- + \text{NO}_2^-$) or from the appearance of N_2 and changes in isotopic composition. Further, we calculated the separate ϵ for NO_3^- reduction to NO_2^- and NO_2^- reduction to N_2 of ~16-21‰ and ~12‰, respectively, when the effect of NO_2^- oxidation could be removed. These results, together with the relationship between N and O of NO_3^- isotopes and the difference in $\delta^{15}\text{N}$ between NO_3^- and NO_2^- , confirm a role for NO_2^- oxidation in increasing the apparent ϵ associated with NO_3^- reduction. The lower ϵ for NO_3^- and NO_2^- reduction as well as N-loss calculated in this study could help reconcile the current imbalance in the global N budget if they are representative of OMZ N-loss.

1. Introduction

Bioavailable fixed nitrogen (N) is an essential macronutrient for phytoplankton that limits marine primary productivity throughout much of the surface ocean. The interplay between sources, mainly N₂ fixation by diazotrophic organisms and sinks, i.e. denitrification and anammox, controls the ocean's fixed N inventory. N sinks occur under low oxygen (O₂) conditions (typically $\leq 5 \mu\text{mol L}^{-1}$) through the conversion of fixed N to predominately N₂ with a small proportion to N₂O, a potent greenhouse gas. It is still a matter of debate whether the global ocean N cycle is in balance at present (Gruber, 2004; 2008, Codispoti, 2007, DeVries et al., 2013). Codispoti (2007) suggested significant imbalances despite huge uncertainties in rate estimates, with more sedimentary and water-column N-loss than N₂ fixation, which would globally impact primary productivity over time and, ultimately, the capacity of phytoplankton to sequester CO₂ in the ocean. While Großkopf et al. (2012) suggested that N₂ fixation rates by direct measurements might have been significantly underestimated, their revised N₂ fixation rates are still insufficient to balance global N-loss in Codispoti (2007)'s budget.

A large portion of the ocean's fixed (i.e. bioavailable) N-loss to N₂ gas takes place in oxygen minimum zones (OMZs) of the eastern tropical North and South Pacific (ETNP and ETSP) and the Arabian Sea, even though they represent only ~1% (O₂ $\leq 20 \mu\text{mol L}^{-1}$) of the total oceanic volume (Lam and Kuypers, 2011). These regions are characterized by high primary productivity and low O₂ supply from source waters. Recent observations suggest an intensification of the world's OMZs over the past few decades (Stramma et al., 2010) and perhaps into the future as a consequence of global warming (Keeling and Garcia, 2002), which underscores the need to better constrain the processes and mechanisms that drive N-loss in these regions. There is now geochemical evidence that mesoscale eddies can act as fixed N loss hotspots in OMZ's (Altabet et al., 2012; Stramma et al., 2013). Eddies are

present in all OMZs during all seasons (Chaigneau et al., 2009; Chelton et al., 2011). An eddy frequency of ~40% was estimated for our study region off Peru, confirming the common occurrence of eddies in this area, with maximal activity occurring during austral fall (Chaigneau et al., 2008). Since eddies lead to heterogeneity in OMZ N-loss processes, a re-evaluation of N-loss pathways and rates as well as the impact of eddies on the global N cycle is required. While the exact mechanism of enhanced N-loss in eddies is still largely unclear, near-coastal eddies could transport and concentrate organic material (OM) from highly productive shelf waters as is speculated for the Peru coastal upwelling region (Altabet et al., 2012). As organic matter input is likely limiting for heterotrophic denitrification in OMZ's (Babbin et al., 2014), such transport would enhance N-loss offshore. Alternatively, cyclonic and mode-waters eddies are characterized by the uplifting of the upper thermocline which can inject nutrients into the euphotic zone thereby fueling primary productivity and downward organic matter flux locally (e.g. McGillicuddy et al., 2007).

Uncertainties in estimating global ocean N-loss rates lie in our lack of understanding of both the spatial and temporal variability of these processes as well as estimating the relative contribution from sedimentary N-loss. The ratio of sedimentary versus water-column N-loss is typically constrained using a global isotope mass balance. Only minor isotope fractionation is imparted during N₂ fixation, the $\delta^{15}\text{N}$ from newly fixed N being ~-2 to 0.5‰ (Wada and Hattori, 1976). In contrast, relatively large kinetic isotope effects (ϵ), i.e. the ratio of reaction rate constants of the light versus the heavy isotopologues, have been reported for water-column NO₃⁻ reduction (~20-30‰; Brandes et al., 1998; Voss et al., 2001; Granger et al., 2008) and NO₂⁻ reduction (~15‰; Bryan et al., 1983; Brunner et al., 2013) during denitrification and anammox. The net ϵ of sedimentary NO₃⁻ reduction is generally much lower (generally $\leq 3\%$), mostly due to diffusion limitation (i.e. NO₃⁻ is all consumed within the sediments) (Lehmann et al., 2007; Alkhatib et al., 2012), although a recent study reports

higher values in surface sediments from the coastal Baltic Sea (up to 19‰, Dähnke and Thamdrup, 2013). These processes and isotope effects set the $\delta^{15}\text{N}$ of mean ocean NO_3^- , which represents the bulk of the dissolved inorganic nitrogen ($\text{DIN} = \text{NO}_3^- + \text{NO}_2^- + \text{ammonium (NH}_4^+)$) in the ocean, at $\sim 5\text{‰}$ (Sigman et al., 2009). Based on isotope mass-balance and directly measured or modeled N_2 fixation and N-loss rates, a ratio of at least 3:1 between sedimentary and water-column N-loss has been estimated (e.g. Brandes and Devol, 2002), indicating large imbalances in the global N budget.

Many uncertainties exist in current environmental estimates of the overall ϵ associated with OMZ N-loss. Some recent studies suggest a lower than canonical value ϵ at the organism-level for NO_3^- reduction during water-column denitrification in OMZ's (Kritee et al., 2012; Casciotti et al., 2013) or lower overall ϵ for N-loss due to local large NO_3^-

drawdown and the contribution from organic N via remineralization and anammox to N_2 production (Altabet, 2007). A lower overall ϵ for OMZ N-loss could reduce current estimates of sedimentary denitrification and thus bring the global N budget more in balance.

Here we address several limitations in previous studies. First, all prior studies have been only able to examine substrate pools (mainly NO_3^-) and could not resolve the relatively small variations expected (due to the large atmospheric background) in the isotopic composition of the product N_2 . Second, Rayleigh equations are typically used to calculate ϵ based on observed changes in isotopic composition as a function of fractional substrate drawdown (f). To determine f , it is necessary to know the DIN expected (N_{exp}) in the absence of N-loss, or initial NO_3^- :

$$f = \text{N}_{\text{obs}} / \text{N}_{\text{exp}}$$

1

The DIN deficit (N_{def}) then is a measure of the amount of fixed N converted to N_2 ;

$$N_{\text{def}} = N_{\text{exp}} - N_{\text{obs}}$$

2

N_{exp} is typically calculated assuming the Redfield ratio of 16 NO_3^- to 1 phosphate (PO_4^{3-}) in the absence of N-loss and N_{obs} is the [DIN] observed (e.g. Devol et al., 2006; Chang et al., 2010). This assumption is likely to be violated in the near-coastal OMZ environment as significant PO_4^{3-} fluxes can be released from iron and manganese oxyhydroxides under anoxic conditions (Wallmann, 2010; Reed et al., 2011). Third, complications from water-mass mixing can also confound estimates if they vary in end-member composition.

Other assumptions usually include identification of dominant N cycle processes. The dual NO_3^- (N and O) isotopic composition can be used to disentangle NO_3^- consumption and production processes in marine environments (Lehmann et al., 2005; Sigman et al., 2005; Bourbonnais et al., 2009; 2013, Casciotti, 2009). NO_3^- consumption by autotrophic uptake or dissimilatory reduction generally fractionate N and O isotopes equally with a $^{15}\epsilon:^{18}\epsilon$ of 1 (Granger et al., 2004; 2008). In contrast, the $\delta^{15}\text{N}$ and $\delta^{18}\text{O}$ of NO_3^- are affected differentially during NO_3^- generation such as remineralization/nitrification of organic material leading to a decoupling of N and O NO_3^- isotopes (i.e. deviation from a 1:1 relationship), when there is simultaneous NO_3^- consumption and production as explained in more detail below (section 3.3.1.2). Parallel measurement of the isotopic composition of NO_2^- further evaluates the influence of NO_2^- oxidation. NO_2^- oxidation to NO_3^- , even at low or non-detectable $[\text{O}_2]$, has been proposed to explain differences in co-occurring $\delta^{15}\text{N-NO}_3^-$ and $\delta^{15}\text{N-NO}_2^-$ (up to ~40‰) that are much larger than expected from NO_3^- reduction alone (Casciotti and McIlvin, 2007, Casciotti et al., 2013). This follows from NO_2^- oxidation incurring an unusual inverse kinetic ϵ (-13 to -31‰, i.e. the residual NO_2^- is depleted in ^{15}N), caused by the reversibility of NO_2^- oxidation at the enzymatic level (Casciotti, 2009).

In this study, we measured NO_3^- , NO_2^- and biogenic N_2 isotopes across a mesoscale eddy in the Peru OMZ during two research cruises in November and December 2012 and located

in deep waters adjacent to the continental slope (Fig. 1). As an anticyclonic mode-water eddy, shallow isopycnal surfaces shoaled and denser surfaces deepened toward its center resulting in an interior of fairly homogenous hydrographic properties (McGillicuddy et al., 2007). We exploited this eddy, with its simplified history and hydrography as well as intense N-loss signals, as a natural tracer experiments to better constrain the net environmental ϵ of N-loss in OMZ's (see Fig. 2 for the terminology used to define the different ϵ estimated in this study). We also used the dual isotopic compositions (N and O) of NO_3^- and NO_2^- to investigate the impact of NO_2^- oxidation on these isotope effects.

2. Sample collection and methods

2.1. Sampling regime and hydrographic data

The impact of mesoscale eddies on the Peru OMZ were studied during two research cruises aboard the RV Meteor on 24 to 25 November (M90) and 22 to 24 December (M91) 2012 (Fig. 1), as part of the German projects SFB 754 (Climate-Biogeochemistry Interactions in the Tropical Ocean: www.sfb754.de) and SOPRAN (Surface Ocean Processes in the Anthropocene: www.sopran.pangaea.de). The presence and locations of the several eddies surveyed were confirmed by satellite data for sea surface height anomaly (SSHA; Fig. 1), sea surface temperature, and chlorophyll α (Stramma et al., 2013). In this study, we only consider the most coastal anticyclonic, mode-water eddy observed during both cruises (corresponding to eddy A in Stramma et al., 2013), to investigate the ϵ of N-loss because it had the most intense N-loss signals (Stramma et al., 2013).

Water samples were collected at every station close to or within the eddy (transects shown in Fig.1) using 12 L Niskin bottles (~23 depths/profile) on a CTD rosette equipped with pressure, conductivity, temperature and O_2 sensors. Oxygen and nutrients (NO_3^- , NO_2^- , NH_4^+ and PO_4^{3-}) concentrations were measured onboard as described in Stramma et al.

(2013). N_{def} was calculated according to equation 2 where N_{exp} was calculated as in Chang et

al. (2010):

$$N_{\text{exp}} = 15.8 \times ([\text{PO}_4^{3-}] - 0.3) \quad 3$$

which takes into account preformed N_{def} in the eastern tropical South Pacific Ocean.

Samples for N and O isotopic composition of NO_3^- were collected in 125 mL plastic bottles and acidified for preservation (1 mL of 2.5 mM sulfamic acid in 25% HCl). Any NO_2^- present in these samples was removed by the sulfamic acid (Sigma S-5643) at a final concentration of $20 \mu\text{mol L}^{-1}$ at the time of sample collection (Granger and Sigman, 2009).

For NO_2^- isotopic analysis, a separate set of samples was collected and preserved with NaOH (2.25 mL of 6M NaOH in 125 mL, pH=12.5) and frozen upon analysis to prevent oxygen isotope exchange with water during storage (Casciotti et al., 2007). N_2/Ar and $\delta^{15}\text{N}-\text{N}_2$ samples were collected in 60 mL serum glass bottles and preserved with 100 μL HgCl_2 (Charoenpong et al., 2014). Duplicate or triplicate samples were collected either at all stations (M90) or every other station (M91).

2.2. N and O isotopic composition of dissolved inorganic N

The stable isotopic compositions ($\delta^{15}\text{N}$ and $\delta^{18}\text{O}$) of NO_3^- and NO_2^- were analyzed using the “azide method” as described in McIlvin and Altabet (2005), with 10% of the total number of samples analyzed as duplicates. For NO_3^- isotopic analysis, cadmium was first used for the reduction of NO_3^- to NO_2^- . For both NO_3^- and NO_2^- isotopic analysis, NO_2^- was converted to nitrous oxide (N_2O) using sodium azide in acetic acid. N_2O gas was automatically extracted, purified, and analyzed on-line using a purge-trap preparation system coupled to an IsoPrime continuous-flow, isotope ratio mass spectrometer (CF-IRMS). The target sample and standard size was 15 nmol N_2O . N and O isotope ratios are reported in per mil (‰), relative to N_2 in air for $\delta^{15}\text{N}$:

$$\delta^{15}\text{N} = (\text{R}_{\text{sample}}/\text{R}_{\text{AIR}} - 1) \times 1000 \quad 4$$

where $\text{R} = {}^{15}\text{N}/{}^{14}\text{N}$, and relative to Vienna Standard Mean Ocean Water (V-SMOW) for $\delta^{18}\text{O}$:

$$\delta^{18}\text{O} = (\text{R}_{\text{Sample}}/\text{R}_{\text{V-SMOW}} - 1) \times 1000$$

5

where $\text{R} = {}^{18}\text{O}/{}^{16}\text{O}$. Isotope values were calibrated using the following international references: IAEA N3 ($\delta^{15}\text{N}=4.7\text{‰}$ and $\delta^{18}\text{O}=25.6\text{‰}$), USGS 34 ($\delta^{15}\text{N}=-1.8\text{‰}$ and $\delta^{18}\text{O}=-27.9\text{‰}$), USGS 35 ($\delta^{15}\text{N}=2.7\text{‰}$ and $\delta^{18}\text{O}=57.5\text{‰}$) and an in-house standard (LABmix, $\delta^{15}\text{N}=38.9\text{‰}$) for NO_3^- isotopic analysis. For NO_2^- isotopic analysis, we used several in-house (MAA1, $\delta^{15}\text{N}=-60.6\text{‰}$; MAA2, $\delta^{15}\text{N}=3.9\text{‰}$; Zh1, $\delta^{15}\text{N}=-16.4\text{‰}$) and other standards (N23, $\delta^{15}\text{N}=3.7\text{‰}$ and $\delta^{18}\text{O}=11.4\text{‰}$; N7272, $\delta^{15}\text{N}=-79.6\text{‰}$ and $\delta^{18}\text{O}=4.5\text{‰}$); N10219, $\delta^{15}\text{N}=2.8\text{‰}$ and $\delta^{18}\text{O}=88.5\text{‰}$; see Casciotti and McIlvin, 2007). Reproducibility was generally better than 0.2‰ for $\delta^{15}\text{N}$ and 0.5‰ for $\delta^{18}\text{O}$.

2.3. N_2/Ar and $\delta^{15}\text{N}-\text{N}_2$ measurements

High precision measurements of N_2/Ar and $\delta^{15}\text{N}-\text{N}_2$ were made on septum sealed samples using on-line gas extraction system coupled to a multicollector CF-IRMS as described in Charoenpong et al. (2014). O_2 was removed from the samples prior to $\delta^{15}\text{N}-\text{N}_2$ analysis using a CuO/Cu reduction column placed in a 500°C furnace to prevent interferences caused by interaction between O_2 , N_2 and their fragments within the IRMS ion source. Excess N_2 concentration ($[\text{N}_2]_{\text{excess}}$) in $\mu\text{mol L}^{-1}$, the observed $[\text{N}_2]$ minus the equilibrium $[\text{N}_2]$ at *in-situ* temperature and salinity, was calculated as in Charoenpong et al. (2014) and calibrated daily against seawater standards equilibrated with air at fixed temperature. Excess N_2 concentrations determined using the O_2 and no O_2 modes agreed well and the average is reported here. Precision of the measurements (standard deviation) for the samples was generally better than $0.7 \mu\text{mol L}^{-1}$ for $[\text{N}_2]_{\text{excess}}$ and 0.03‰ for $\delta^{15}\text{N}-\text{N}_2$.

2.4 Derived parameter calculations

2.4.1. $\Delta(15,18)$ and $\Delta\delta^{15}\text{N}$

We calculated NO_3^- isotope anomalies, i.e. the deviation from a 1:1 relationship

expected during NO_3^- assimilation or denitrification, following Sigman et al. (2005):

$$\Delta(15,18) = \delta^{15}\text{N} - \delta^{15}\text{N}_m - [({}^{18}\epsilon/{}^{15}\epsilon)(\delta^{18}\text{O} - \delta^{18}\text{O}_m)] \quad 6$$

where $\delta^{15}\text{N}_m = 5.5\text{‰}$ and $\delta^{18}\text{O}_m = 2.5\text{‰}$ are the mean $\delta^{15}\text{N}$ and $\delta^{18}\text{O}$ values of the deep waters for this region (this study and Casciotti et al., 2013) and ${}^{18}\epsilon/{}^{15}\epsilon$ is the ratio of N versus O isotope enrichment of 1:1 observed during assimilatory or dissimilatory NO_3^- reduction (Granger et al., 2004; 2008, Lehmann et al., 2005). $\Delta\delta^{15}\text{N}$, defined as the difference between $\delta^{15}\text{N}-\text{NO}_3^-$ and $\delta^{15}\text{N}-\text{NO}_2^-$ (Casciotti et al., 2013), was calculated when $\delta^{15}\text{N}-\text{NO}_2^-$ data were available.

2.4.2. Biogenic N_2 and $\delta^{15}\text{N}-\text{N}_2$

We calculated biogenic $[\text{N}_2]$ ($[\text{N}_2]_{\text{biogenic}}$), the $[\text{N}_2]$ produced by denitrification or anammox, by subtracting the $[\text{N}_2]_{\text{excess}}$ at a background station unaffected by N-loss ($[\text{O}_2] > 10 \mu\text{mol L}^{-1}$) located north of the OMZ (1.67°N, 85.83°W, M90 cruise) from the observed $[\text{N}_2]_{\text{excess}}$ at corresponding σ_θ (see supplementary material S1). This corrects for non-local biological N-loss as well as physically-produced deviations in equilibrium N_2/Ar (e.g. bubble injection at remote water mass outcrop regions, see Hamme, 2002).

The $\delta^{15}\text{N}$ of biogenic N_2 ($\delta^{15}\text{N}-\text{N}_2_{\text{biogenic}}$, in ‰) was calculated by mass balance:

$$\delta^{15}\text{N}-\text{N}_2_{\text{biogenic}} = [([\text{N}_2]_{\text{equil}} + [\text{N}_2]_{\text{biogenic}}) \times \Delta\delta^{15}\text{N}-\text{N}_2] / [\text{N}_2]_{\text{biogenic}} \quad 7$$

where $[\text{N}_2]_{\text{equil}}$ is the equilibrium $[\text{N}_2]$ at *in-situ* temperature and salinity, and $\Delta\delta^{15}\text{N}-\text{N}_2$ is the $\delta^{15}\text{N}-\text{N}_2$ anomaly, i.e. the difference between $\delta^{15}\text{N}-\text{N}_2$ observed and at equilibrium for *in-situ* temperature and salinity.

We also calculated the expected $\delta^{15}\text{N}$ -biogenic N_2 ($\delta^{15}\text{N}-\text{N}_2_{\text{biogenic exp}}$) from our DIN isotope data to assess isotopic mass balance between DIN loss and $[\text{N}_2]_{\text{biogenic}}$ production (see section 3.2.3):

$$\delta^{15}\text{N-N}_2 \text{ biogenic exp} = [\text{N}_{\text{exp}} \times 5.5 - [\text{NO}_3^-] \times \delta^{15}\text{N-NO}_3^- - [\text{NO}_2^-] \times \delta^{15}\text{N-NO}_2^-] / \text{N}_{\text{def}} \quad 8$$

where 5.5 is the $\delta^{15}\text{N}$ in ‰ of DIN prior to N-loss.

2.5. Isotope effect calculations

We calculated isotope effects first assuming a closed system where there is mass balance between the consumption of NO_3^- or DIN (the sum of NO_3^- and NO_2^-) and the accumulation of biogenic N_2 over time (e.g. no external sources or sinks), using Rayleigh equations:

$$\delta^{15}\text{N}_{\text{substrate}}(f) = \delta^{15}\text{N}_{\text{substrate}}(f=1) - \epsilon \times \ln[f] \quad 9$$

$$\delta^{15}\text{N}_{\text{product}}(f) = \delta^{15}\text{N}_{\text{substrate}}(f=1) + \epsilon f/[1-f] \times \ln[f] \quad 10$$

where f is the fraction of remaining NO_3^- or DIN.

In addition, we calculated isotope effects assuming a steady-state open system, as is the case where the substrate is continually replenished by mixing, using modified Rayleigh equations (Mariotti et al., 1981; Altabet, 2005):

$$\delta^{15}\text{N}_{\text{substrate}}(f) = \delta^{15}\text{N}_{\text{substrate}}(f=1) + \epsilon \times [1-f] \quad 11$$

$$\delta^{15}\text{N}_{\text{product}}(f) = \delta^{15}\text{N}_{\text{substrate}}(f=1) - \epsilon \times f \quad 12$$

f was calculated for NO_3^- (f_1) or DIN removal (f_2) by either 1) assuming Redfield stoichiometry to calculate the initial $[\text{NO}_3^-]$ or $[\text{DIN}]$ (see eq. 2):

$$f_{1\text{-red}} = [\text{NO}_3^-]_{\text{obs}} / [\text{N}]_{\text{exp}} \quad 13$$

$$f_{2\text{-red}} = [\text{NO}_3^- + \text{NO}_2^-]_{\text{obs}} / [\text{N}]_{\text{exp}} \quad 14$$

or 2) by using the sum of observed $[\text{DIN}]$ and $[\text{N}_2]_{\text{biogenic}}$:

$$f_{1\text{-bN}_2} = [\text{NO}_3^-]_{\text{obs}} / ([\text{NO}_3^-]_{\text{obs}} + [\text{NO}_2^-]_{\text{obs}} + [\text{N}_2]_{\text{biogenic}} \times 2) \quad 15$$

$$f_{2\text{-bN}_2} = [\text{NO}_3^- + \text{NO}_2^-]_{\text{obs}} / ([\text{NO}_3^-]_{\text{obs}} + [\text{NO}_2^-]_{\text{obs}} + [\text{N}_2]_{\text{biogenic}} \times 2) \quad 16$$

3. Results and discussion

3.1. An eddy N-loss hotspot

The formation of near-coastal eddies south of 15°S off San Juan (Peru) during the austral spring have been associated with a reduction in coastal upwelling and advection of warmer and saltier subtropical waters from the Chile-Peru Undercurrent. Eddy A first appeared on the shelf after 13 September 2012 and was thus about 2 (M90) to 3 (M91) months old at the time of sampling. In November 2012 (M90 cruise), it had already separated from the shelf-break and stayed stationary at ~16°S and ~76°W until mid-December 2012. This anticyclonic eddy was up to 2°C warmer and 0.2 saltier at its center relative to its edges, and had a swirl velocity of up to 35 cm s⁻¹. The vertical density distribution showed lens-shaped isopycnals, characteristic of a mode-water eddy, i.e. the isopycnals were uplifted and deepened above and below 110 m, respectively (Fig. 3). The largest differences in physical and chemical properties between the center and the edges of the eddy were observed in the upper 600 m. Near real time satellite data for November 21, supported by density, velocity, O₂, nutrient and chlorophyll α data, confirmed that the core of the eddy was located at ~76.30°W during the M90 cruise (station 162) though the delayed time SSHA data in Fig. 1a suggest it was located east of the transect used in this study. In mid-December, the eddy started to move northwestward at 6.6 cm s⁻¹ and on 22 to 24 December 2012, during the M91 sampling campaign (see Fig. 1), its core was located at ~16.5°S, ~76.5°W (Stramma et al., 2013). See Stramma et al. (2013) for a more detailed analysis of the physical and chemical properties (e.g. O₂, pH) associated with this near-coastal eddy for the M90 cruise.

Remarkably, NO₃⁻ was completely depleted by N-loss processes near the eddy's center. Concentrations were ~0 $\mu\text{mol L}^{-1}$ in the upper part of the OMZ (between ~50 to 150 m depth) at stations 162 (M90) and 88 (M91; Fig. 4, a, b), and no NO₃⁻ isotope data could be obtained for these depths. As expected during dissimilatory NO₃⁻ reduction (Brandes et al.,

1998; Voss et al., 2001; Granger et al., 2008), NO_3^- $\delta^{15}\text{N}$ and $\delta^{18}\text{O}$ increased to up to $\sim 70\text{‰}$ and $\sim 58\text{‰}$ at ~ 200 m depth with decreasing concentration ($\sigma_\theta = 26.3$). These are the highest values reported to date for marine environments (Fig. 4, c, d, e, f).

$[\text{NO}_2^-]$, produced as an intermediate during NO_3^- reduction, accumulated to up to $\sim 11 \mu\text{mol L}^{-1}$ at 200 to 250 m depth near the core of the eddy (Fig. 5, a, b). $\delta^{15}\text{N-NO}_2^-$ increased to up to $\sim 53\text{‰}$ (60 m depth, M90) and $\sim 26\text{‰}$ (75 m depth, M91) where NO_3^- was completely consumed, consistent with isotopic fractionation during NO_2^- reduction by denitrification and/or anammox. The lowest $\delta^{15}\text{N-NO}_2^-$ values (-31‰ to -34‰) were observed deeper, close to the anoxic/oxic transition at ~ 400 m depth (i.e. station 160, M90; station 89/90, M91), and suggests aerobic or anaerobic NO_2^- oxidation, associated with inverse kinetic isotope effects (Casciotti, 2009; Brunner et al., 2013; Fig. 5, c, d). The $\delta^{18}\text{O-NO}_2^-$ remained fairly constant at $\sim 15\text{‰}$ (Fig. 5, e, f), similar to the value of $+14\text{‰}$ for abiotic NO_2^- oxygen isotope exchange with water at *in situ* temperature reported in Casciotti et al. (2007). This observation implies a residence time for NO_2^- in the eddy of at least several weeks.

Extreme N_{def} (eq. 1) of up to $\sim 44 \mu\text{mol L}^{-1}$ was also observed near the core of the eddy at ~ 50 m depth (Fig. 6, a, b). Biogenic $\text{N}_2\text{-N}$, which is simply $[\text{N}_2]_{\text{biogenic}}$ (see section 2.4.2) multiplied by 2 to facilitate direct comparison with N_{def} , only reached $35 \mu\text{mol L}^{-1}$, but otherwise generally agreed well with N_{def} , within analytical errors, as in Chang et al. (2010; 2012) (Fig. 6, c, d). $\delta^{15}\text{N-N}_2_{\text{biogenic}}$ (eq. 7) ranged from -13.3‰ to 4.6‰ when considering $[\text{N}_2]_{\text{biogenic}} \geq 2 \mu\text{mol L}^{-1}$ (our mean propagated analytical error; Fig. 6, e, f), and increased with decreasing $[\text{NO}_3^-]$, following isotopic fractionation during NO_3^- conversion to NO_2^- and N_2 . The highest $\delta^{15}\text{N-N}_2_{\text{biogenic}}$ value (4.6‰) was observed near the core of the eddy at ~ 80 m depth during the M90 cruise. This high $\delta^{15}\text{N-N}_2_{\text{biogenic}}$ was consequently associated with complete NO_3^- consumption, low residual NO_2^- ($\sim 0.6 \mu\text{mol L}^{-1}$), and the highest $\delta^{15}\text{N-NO}_2^-$ and was similar to mean $\delta^{15}\text{N-NO}_3^-$ ($\sim 5\text{‰}$) in the ocean.

Altabet et al. (2012) interpreted unusually high N-loss at one station in the Peru OMZ as reflecting stimulation by an adjacent eddy. We clearly confirm this finding with our more highly resolved observations of intense N-loss and associated isotopic signals in Eddy A. A chlorophyll α maximum, most likely transported from the coast, was observed during the M90 cruise at the center of the eddy (up to $\sim 6.1 \mu\text{g L}^{-1}$ at ~ 50 m depth; Stramma et al., 2013). It is possible that such transport may be the organic ‘fuel’ for N-loss within the eddy (Altabet et al., 2012). Different studies have attributed N-loss in OMZs to either anammox, fueled by the breakdown of OM to NH_4^+ (Kalvelage et al., 2013), or denitrification (Ward et al., 2009). An increase in the quantity of exported OM has recently been found to significantly enhance N-loss (Babbin et al., 2014). In this study, we also observed the most intense N-loss signals near the core of the anticyclonic coastal eddy, where uplifting of isopycnals extended the OMZ into shallower and more productive waters transported from the coast with higher OM content (Stramma et al., 2013). Irrespective of the specific N-loss process at play (i.e. denitrification versus anammox) the large N deficits and extreme isotopic signatures associated with the anticyclonic coastal eddy, coupled with our extensive sampling program, represents an ideal natural tracer experiment to examine, for the first time, the environmental ϵ associated with specific N processing steps (Fig. 2) as well as overall net N-loss ($^{15}\epsilon_{\text{DIN-loss}}$ or $^{15}\epsilon_{\text{N}_2}$, see sections 3.2.1 and 3.2.3) in this OMZ.

3.2. Comparing approaches for evaluating ϵ

Temperature-salinity plots support a single water mass for low- O_2 waters in the eddy (Fig. 3, b, d). Consequently, changes in salinity and temperature for selected isopycnal ranges in Table 1 and 2 were relatively small and this simplified hydrography suggests both a single set of initial conditions and little influence from mixing of distinct water masses. This setting is ideal for applying closed system Rayleigh equations for calculating ϵ . Nevertheless, rapid mixing along isopycnal surface may not be reflected in the T-S diagram and would result in

underestimates of ϵ using the closed system approach. Alternatively, the Rayleigh open system model mimics the effects of mixing as a mechanism for continual resupply of NO_3^- (Altabet, 2005; also see section 2.5). Below, we compare closed and open system approaches for estimating ϵ using both source ($\delta^{15}\text{N-DIN}$) and product ($\delta^{15}\text{N-N}_2$ biogenic) versions of these equations as a double check. We also take advantage of eddy's simple hydrography (one end-member) to test the assumption of Redfield stoichiometry for calculating f by comparison with f based on $[\text{N}_2]_{\text{biogenic}}$ (f_{red} vs f_{bN_2}). Last, to consider overall isotope fractionation effects, we calculate apparent ϵ using f values based on NO_3^- removal (f_1) and DIN removal (f_2) (equations 9, 11) in comparison to ϵ based on the changes in $\delta^{15}\text{N-N}_2$ biogenic (equations 10, 12).

3.2.1. Comparing ϵ for closed versus open systems

First we examine the apparent ϵ associated with the disappearance of NO_3^- ($^{15}\epsilon_{\text{NO}_3^- \text{red}}$, Fig. 2). Assuming a Rayleigh closed system model, $^{15}\epsilon_{\text{NO}_3^- \text{red}}$ significantly increased (p-value < 0.05, t-test) from 12‰ for the shallowest potential density range ($26.2 < \sigma_\theta \leq 26.3$) to up to 24‰ ($26.3 < \sigma_\theta \leq 26.5$) and then to up to 31‰ closer to the anoxic/oxic transition zone deeper in the water column ($26.5 < \sigma_\theta \leq 26.8$) for the M90 transect (Table 1). No such clear relationship was observed for the M91 transect, although the highest $^{15}\epsilon_{\text{NO}_3^- \text{red}}$ (26‰) was also observed for a higher potential density range of $26.5 > \sigma_\theta \leq 26.7$. NO_3^- assimilation by phytoplankton in the OMZ, with a ϵ of ~ 5 ‰ (Altabet, 2001), could lower the ϵ for shallower potential density range in the ETSP. We still observed lower than expected $^{15}\epsilon_{\text{NO}_3^- \text{red}}$, despite only using data points deeper than 100 m (the peak in chlorophyll α being at ~ 50 m depth) to minimize NO_3^- assimilation effects (Table 1). One explanation could be partial suppression of the $^{15}\epsilon_{\text{NO}_3^- \text{red}}$ at low $[\text{NO}_3^-]$ within the OMZ as the system approached nearly complete substrate consumption (NO_3^- and NO_2^-), as suggested by previous studies (Granger et al.,

2008; Kritee et al., 2012; Frey et al., 2014). However, the onset of this asymptotic behavior was observed in this study at lower substrate concentrations ($[\text{NO}_3^-]$ or $([\text{NO}_3^-] + [\text{NO}_2^-]) < \sim 13 \mu\text{mol L}^{-1}$) as compared to the threshold of $\sim 35 \mu\text{mol L}^{-1}$ reported by Kritee et al. (2012) for laboratory experiments. Depressed ε at low $[\text{NO}_3^-]$ was explained by these authors as a decrease in NO_3^- efflux into the microbial periplasm relative to the fraction of gross NO_3^- uptake into the cell where it is reduced to NO_2^- by the membrane-bound NO_3^- reductase (*Nar*). *Nar* has been identified as being responsible for the majority of cellular NO_3^- reduction and is the dominant driver of isotope enrichment during denitrification (Granger et al., 2008). We thus only considered the linear portion of the relationship ($[\text{NO}_3^-]$ or $([\text{NO}_3^-] + [\text{NO}_2^-]) > 13 \mu\text{mol L}^{-1}$, $\sigma_\theta > 26.3$), which represented >80-90% of the data, to estimate the overall $^{15}\varepsilon_{\text{NO}_3\text{-red}}$ or $^{15}\varepsilon_{\text{DIN-loss}}$ (see below) in the OMZ (Fig. 7, a, b). We estimated a overall $^{15}\varepsilon_{\text{NO}_3\text{-red}}$ for Eddy A of $\sim 20\%$, with no significant difference between the M90 and M91 transects (Table 1), which is in the lower range of $^{15}\varepsilon_{\text{NO}_3\text{-red}}$ from previous studies (20-30%, Brandes et al., 1998; Voss et al., 2001; Granger et al., 2008).

The unrealistically high $^{15}\varepsilon_{\text{NO}_3\text{-red}}$ (up to 128‰), as well as the extremely low intercept (down to -63‰, which should equal the initial $\delta^{15}\text{N}$ of the substrate, see equation 11), calculated for the shallowest potential density ranges suggest the inadequacy of the open system model, especially at low $[\text{NO}_3^-]$, in this setting. Overall $^{15}\varepsilon_{\text{NO}_3\text{-red}}$ was twice as high for the open system model ($\sim 40\%$, for both M90 and M91 transects; Table 2). A higher ε for an open system scenario is expected since NO_3^- with a low $\delta^{15}\text{N}$ is assumed to be continuously re-supplied, thus ε must be larger to account for the observed isotopic enrichment.

Using DIN as the basis to calculate ϵ ($^{15}\epsilon_{\text{DIN-loss}}$, see Fig. 2), while not representative of NO_3^- reduction per se, provides better estimates of overall isotope fractionation for N-loss, and is more comparable to ϵ calculated using $\delta^{15}\text{N-N}_2$ biogenic. f_{bN_2} was used in the Rayleigh equations and $\delta^{15}\text{N}$ was calculated from the concentration-weighted average $\delta^{15}\text{N-DIN}$ (from $\delta^{15}\text{N-NO}_3^-$ and $\delta^{15}\text{N-NO}_2^-$ values). The overall $^{15}\epsilon_{\text{DIN-loss}}$ estimated using a closed system model (13‰, Fig. 7, a, b) was also significantly lower than for an open system model (19‰), and also showed no significant difference between transects (Tables 1 and 2). Lower $^{15}\epsilon_{\text{DIN-loss}}$ values (down to 4.5‰) were also observed for $\sigma_\theta < 26.3$ in the OMZ, where $[\text{NO}_3^-]$ was significantly depleted. No significant variation with potential density ranges could be discerned deeper in the water column. These two models are extreme scenarios, and intermediate (e.g. partial) mixing regimes, would yield $^{15}\epsilon_{\text{DIN-loss}}$ between these two values (e.g. Sigman et al., 2003). Partial mixing is unlikely to occur in anticyclonic eddies where evidence for enhanced mixing has been found (e.g. see Kunze et al., 1995).

3.2.2. Testing the assumption of Redfield stoichiometry for estimating N_{exp}

Most previous studies have assumed Redfield stoichiometry with PO_4^{3-} to estimate initial NO_3^- (N_{exp}), a key term for determining f and thus $^{15}\epsilon_{\text{NO}_3\text{-red}}$ or $^{15}\epsilon_{\text{DIN-loss}}$. We suspect that assumption of Redfield stoichiometry may fail in our setting since PO_4^{3-} can be preferentially liberated (Wallmann, 2010; Reed et al., 2011) and these fluxes could be transported offshore especially in the case of our near-coastal eddy. Excess PO_4^{3-} would result in overestimation of N_{exp} .

Here we test the validity of this assumption by comparing ϵ values calculated using this approach with those calculated using our biogenic N_2 data to estimate N_{exp} (see eq. 13 to 16). For simplicity, we show calculation results only for a closed system (eq. 9, 10). We find that no significant difference could be discerned for $^{15}\epsilon_{\text{NO}_3\text{-red}}$ or $^{15}\epsilon_{\text{DIN-loss}}$ calculated using

either approach (Table 1). These results are not completely surprising considering the general agreement between N deficit and biogenic N_2 -N (Fig. 6, a-d), as also reported in Chang et al. (2010; 2012) for the ETSP and ETNP OMZs. We thus conclude that, at least in offshore waters of the ETSP, both approaches, i.e. calculating N_{exp} from $[PO_3^{4-}]$ assuming Redfield stoichiometry or using the sum of observed $[DIN]$ and $[N_2]_{\text{biogenic}}$ (from measured N_2/Ar data) are equally valid.

3.2.3. Comparing ϵ calculated from the $\delta^{15}N$ of substrate (NO_3^- or DIN) versus product (biogenic N_2)

Prior studies have estimated the ϵ for N-loss solely from $\delta^{15}N$ variations in the substrate (mainly NO_3^- pool). $\delta^{15}N$ variations in N_2 have not been so used due to the weak isotopic signals caused by high background $[N_2]$ dissolved in seawater ($\sim 500 \mu\text{mol L}^{-1}$) as compared to $[N_2]_{\text{biogenic}}$ (typically $\leq 20 \mu\text{mol L}^{-1}$), leading to large errors in the $\delta^{15}N$ - N_2 biogenic calculation. Furthermore, Charoenpong et al. (2014) showed that the presence of O_2 can cause isobaric interferences within the ion source, appreciably compromising the precision and accuracy of $\delta^{15}N$ - N_2 measurements. The high precision of our analytical method, which removes these interferences (0.03‰ for $\delta^{15}N$ - N_2 , see Charoenpong et al., 2014), as well as the high $[N_2]_{\text{biogenic}}$ produced in the eddy, allowed us to also estimate the ϵ for the overall net N-loss from the $\delta^{15}N$ of the product pool ($^{15}\epsilon_{bN_2}$ eq. 10, 12).

Before making this comparison, we first assess that the system is in isotopic balance to ensure that there were no unidentified N sources or sinks. Expected $\delta^{15}N$ for biogenic N_2 is calculated from the change in DIN and its $\delta^{15}N$. Isotope mass balance is confirmed by a 1:1 relationship between measured and expected $\delta^{15}N$ - N_2 biogenic (Fig. 7, e and f, eq. 8). Evidently, biogenic N_2 almost completely originates from the DIN pool, with small discrepancies associated with OM remineralization. These results challenge the conclusion in Kalvelage et al. (2013) for the Peru OMZ that NH_4^+ for anammox, where anammox dominates N-loss,

must derive primarily from organic matter remineralization. The observed isotopic mass balance further implies that, if anammox is important, most of the NH_4^+ pool must rather be derived from the DIN pool, i.e. dissimilative NO_3^- reduction to NH_4^+ (DNRA), as previously suggested by Lam et al. (2009).

For comparing ϵ values calculated using either substrate or product $\delta^{15}\text{N}$, we only consider data points where $[\text{N}_2]_{\text{biogenic}}$ was $\geq 7.5 \mu\text{mol L}^{-1}$ (corresponding to $26.0 > \sigma_0 < 26.5$), since considerably more noise was associated with lower $[\text{N}_2]_{\text{biogenic}}$ due to the dilution effect with background N_2 . We estimate an overall $^{15}\epsilon_{\text{bN}_2}$ of up to 14‰ assuming a closed system (Fig. 7, c, d) and up to 17‰ for an open system, with no significant difference between transects (Tables 1 and 2). These $^{15}\epsilon_{\text{bN}_2}$ values were not significantly different (t-test, p-value < 0.05) from the overall $^{15}\epsilon_{\text{DIN-loss}}$ (13‰ and 19‰ for closed and open systems, respectively), as supported by our isotope mass balance.

Our results directly confirm, for the first time in a natural setting, a lower overall ϵ for net N-loss than previously assumed in OMZs, at least in the ETSP, and support the relatively low ϵ for NO_3^- reduction of 12‰ modeled by Casciotti et al. (2013) for this region. Deutsch et al. (2004) previously discussed how mixing of denitrified water with waters with high $[\text{NO}_3^-]$ from outside the OMZ can yield an artificially low ϵ because of “the dilution effect”, i.e. the $\delta^{15}\text{N}$ of NO_3^- of the resulting mixture is biased toward the water with the highest $[\text{NO}_3^-]$, especially in regions where N-loss is intensified. However, our examination of an eddy N-loss hotspot of only ~100 km diameter makes unlikely the significance of such an effect for our estimates. The difference between our observations and canonical values reflects the interplay between the processes schematized in Fig. 2, though other factors not investigated in this study could also affect the ϵ of N-loss. For example, autotrophic denitrification, possibly coupled to H_2S oxidation (i.e. a cryptic sulfur cycle, see Canfield et al. (2010)),

could incur low process-specific isotope fractionation, as suggested by Wenk et al. (2014).

Our results have important implications and could bring the global N budget closer to being in balance if general for OMZ N-loss. For instance, a lower ϵ for N-loss implies that, at steady state, a significantly lower proportion of sedimentary denitrification, generally associated with little isotopic fractionation, is required to explain the constant average oceanic $\delta^{15}\text{N}$ of $\sim 5\%$, (see Altabet, 2007).

3.2.4. ϵ for NO_2^- removal ($^{15}\epsilon_{\text{NIR}}$)

The ϵ associated with NO_2^- reduction has been poorly constrained, with current estimates varying between 0% (at low $[\text{NO}_2^-]$ and reduction rates) and up to 25% for laboratory denitrifying bacteria cultures (Bryan et al., 1983) and 15% for anammox bacteria (Brunner et al., 2013). Until now, there have been no field-based estimates from OMZ's.

Within the core of Eddy A, we observed nearly complete NO_3^- consumption as well as strong gradients in NO_2^- concentration and $\delta^{15}\text{N}$ value. These conditions allowed us to rule out influences on NO_2^- $\delta^{15}\text{N}$ from either continued NO_3^- reduction to NO_2^- or NO_2^- oxidation to NO_3^- in this sub-region of Eddy A. The observed large excursions in $\delta^{15}\text{N}\text{-NO}_2^-$ in this sub-region could thus only be attributed to NO_2^- reduction, which allowed us to better constrain its environmental ϵ ($^{15}\epsilon_{\text{NIR}}$, Fig. 2). We approximated an $^{15}\epsilon_{\text{NIR}}$ of $\sim 12\%$ from the relationship between $\delta^{15}\text{N}\text{-NO}_2^-$ and $\ln [\text{NO}_2^-]$ (Fig. 8), which is within the range of previous laboratory estimates. This approach assumes the highest $[\text{NO}_2^-]$ observed as the initial concentration for all points considered and resulted in the same slope as the relationship between $\delta^{15}\text{N}\text{-NO}_2^-$ and $\ln ([\text{NO}_2^-]/[\text{NO}_2^-_{\text{max}}])$ (Mariotti et al., 1981).

3.3. Factors influencing observed ϵ

3.3.1. Effects of NO_2^- oxidation

We evaluated the effect of NO_2^- oxidation on the $^{15}\epsilon_{\text{NO}_3^- \text{ red}}$ by estimating ϵ in the absence of NO_2^- , which precludes concurrent NO_2^- oxidation, then considered the additional information provided by $\Delta(15,18)$ and $\Delta\delta^{15}\text{N}$, and compared our values with modeling results and data previously presented by Casciotti et al. (2013) for the same region.

3.3.1.1. $^{15}\epsilon_{\text{NO}_3^- \text{ red}}$ without the influence of NO_2^- oxidation ($^{15}\epsilon_{\text{NAR}}$)

Canonically, the first step in OMZ N-loss is irreversible NO_3^- reduction to NO_2^- (Fig. 2). If so, ϵ for this first step, $^{15}\epsilon_{\text{NAR}}$, should set the overall ϵ for end N-loss and no difference should be observed between $^{15}\epsilon_{\text{NAR}}$ and $^{15}\epsilon_{\text{DIN-loss}}$ or $^{15}\epsilon_{\text{N}_2}$. Recently, significant rates of NO_2^- oxidation back to NO_3^- have been observed in OMZ's despite low or below detection [O_2] (Füssel et al., 2011), which provides a likely explanation for our observation of high $^{15}\epsilon_{\text{NO}_3^- \text{ red}}$ as compared to $^{15}\epsilon_{\text{DIN-loss}}$ or $^{15}\epsilon_{\text{N}_2}$. An unusual inverse kinetic ϵ of -13‰ has been identified for aerobic NO_2^- oxidation (Casciotti, 2009) which results in isotopic enrichment of the product NO_3^- and depletion in the substrate NO_2^- . Anaerobic NO_2^- oxidation by anammox bacteria is also associated with an inverse kinetic ϵ of -31‰. (Brunner et al., 2013). The net effect would be to increase the $^{15}\epsilon_{\text{NO}_3^- \text{ red}}$ since in this case it would be a function of the individual ϵ for NO_3^- reduction alone ($^{15}\epsilon_{\text{NAR}}$) and NO_2^- oxidation as previously suggested by a modeling experiment by Casciotti et al. (2013) in the OMZ of the ETSP.

We obtained significantly lower $^{15}\epsilon_{\text{NAR}}$ of 16‰ for closed system and 21‰ for open system equations by only considering data points with $[\text{NO}_2^-] < 0.05 \mu\text{mol L}^{-1}$ (Fig. 9).

Our $^{15}\epsilon_{\text{NAR}}$ of 16‰ assuming a closed system is more similar to the ϵ of 10-15‰ for cellular-level denitrification at low $[\text{NO}_3^-]$ (2-35 $\mu\text{mol L}^{-1}$) measured by Kritee et al. (2012) in a controlled laboratory experiment or the ϵ for NO_3^- reduction of 12‰ from modeling results in the OMZ off Peru by Casciotti et al. (2013). Diverse $^{15}\epsilon_{\text{NAR}}$ values have also been reported

for different strains of denitrifiers using different types of NO_3^- reductase (i.e. *NAR* versus *NAP*), with lower $^{15}\epsilon$ (i.e. 8 to 13‰) observed when NO_3^- reduction is mediated by *NAP* (Granger et al., 2008). This contrast with values of up to 31‰ (closed system) in the presence of NO_2^- in this study and indicate that NO_2^- oxidation indeed increases apparent $^{15}\epsilon_{\text{NO}_3^- \text{ red.}}$.

3.3.1.2. Evidence from coupled NO_3^- N and O isotopes

NO_3^- N and O isotopes are useful to separate NO_3^- consumption and production processes in marine environments (Granger et al., 2004; 2008; Lehmann et al., 2005; Sigman et al., 2005; Bourbonnais et al., 2009; 2013). Assimilative or dissimilative NO_3^- consumption generally fractionates N and O isotopes equally, with a relationship between $\delta^{18}\text{O}-\text{NO}_3^-$ versus $\delta^{15}\text{N}-\text{NO}_3^-$ ($^{18}\epsilon: ^{15}\epsilon$) of 1 (Granger et al., 2004; 2008). Deviation from a 1:1 ratio for $^{18}\epsilon: ^{15}\epsilon$ (0.60-0.70) were observed during NO_3^- reduction by the periplasmic *NAP* NO_3^- reductase. However, as mentioned previously, *NAR* (with a $\Delta^{18}\text{O}:\Delta^{15}\text{N}$ of ~ 1) was identified as the main driver for isotope fractionation (Granger et al., 2008). In contrast, the $\delta^{15}\text{N}$ and $\delta^{18}\text{O}$ of NO_3^- are independently set during production processes. The $\delta^{15}\text{N}$ of NO_3^- added by nitrification is set by the $\delta^{15}\text{N}$ of the organic matter being remineralized whereas the $\delta^{18}\text{O}$ depends on the ϵ during NH_4^+ and NO_2^- oxidation, water incorporation (with $\delta^{18}\text{O}-\text{H}_2\text{O}$ of $\sim 0\text{‰}$) and the exchange of oxygen atoms with water, that should generate a $\delta^{18}\text{O}$ of newly produced NO_3^- between -8 to -1‰ (Buchwald and Casciotti, 2010). However, the $\delta^{18}\text{O}$ of NO_3^- throughout the deep ocean and away from regions of biological NO_3^- depletion is typically 2 to 3‰ (e.g. Sigman et al., 2005; Bourbonnais et al., 2009). In any case, the $\delta^{18}\text{O}$ of newly generated NO_3^- is not affected by the source of N being nitrified, be it OM from N_2 fixing or other NH_4^+ assimilating organisms or denitrified NO_2^- . Negative N-to-O NO_3^- isotope anomalies, the deviation from a 1:1 relationship for $\delta^{18}\text{O}-\text{NO}_3^-$ and $\delta^{15}\text{N}-\text{NO}_3^-$ during NO_3^- consumption, (see eq. 6), have been interpreted as evidence for a concurrent NO_3^-

source low in $\delta^{15}\text{N}$ (relative to the $\delta^{18}\text{O}-\text{NO}_3^-$) such as N_2 fixation (Sigman et al., 2005; Bourbonnais et al., 2009) or NO_2^- oxidation (Casciotti and McIlvin, 2007; Casciotti et al., 2013).

The effect of rapid cycling of NO_3^- reduction and NO_2^- re-oxidation as compared to N-loss would be to elevate $\delta^{18}\text{O}$ relative to $\delta^{15}\text{N}$ of NO_3^- (Sigman et al., 2005). During NO_3^- reduction, ^{16}O is preferentially lost, and following NO_2^- re-oxidation, an O atom with a higher $\delta^{18}\text{O}$ is incorporated to the newly produced NO_3^- . $\delta^{15}\text{N}-\text{NO}_3^-$ is not expected to change during a cycle of NO_3^- reduction and complete NO_2^- re-oxidation (NO_2^- does not accumulate), therefore generating negative $\Delta(15,18)$. However, incomplete NO_2^- re-oxidation (NO_2^- accumulation) adds high $\delta^{15}\text{N}$, because of the inverse ϵ for NO_2^- oxidation (-13 to -31‰; Casciotti, 2009; Brunner et al., 2013) and can either produce positive or negative $\Delta(15,18)$, depending on the $\delta^{18}\text{O}$ of the O atom added. NO_2^- oxidation can decrease $\delta^{18}\text{O}-\text{NO}_3^-$ relative to $\delta^{15}\text{N}-\text{NO}_3^-$ when ambient $\delta^{15}\text{N}$ and $\delta^{18}\text{O}$ of NO_3^- are higher than ~10-15‰, causing positive $\Delta(15,18)$. The production of negative or positive $\Delta(15,18)$ during NO_2^- oxidation thus depends on the initial NO_3^- and NO_2^- isotopic compositions (Casciotti and Buchwald, 2012; Casciotti et al., 2013).

We obtained a slope >1 (1.4-2.3, $r^2=0.99$) for the relationship between $\delta^{18}\text{O}-\text{NO}_3^-$ versus $\delta^{15}\text{N}-\text{NO}_3^-$ for $[\text{NO}_2^-]<0.05 \mu\text{mol L}^{-1}$ in the OMZ ($[\text{O}_2]<10 \mu\text{mol L}^{-1}$), leading to negative $\Delta(15,18)$ (Fig. 10, a, b). As discussed above, this negative $\Delta(15,18)$ can be caused by a complete cycle of NO_3^- reduction/ NO_2^- re-oxidation. The slope for $[\text{NO}_2^-]\geq 0.05 \mu\text{mol L}^{-1}$ was <1 (0.80, $r^2=0.99$) and crossed the 1:1 line at a $\delta^{15}\text{N}-\text{NO}_3^-$ of ~15‰, which is the threshold suggested by Casciotti et al. (2013) for the production of positive $\Delta(15,18)$. $\Delta(15,18)$ varied from -4.5‰ at 250-400 m depth to up to 9-11‰ at 200 m depth where $\delta^{15}\text{N}$ and $\delta^{18}\text{O}$ of NO_3^- and $[\text{NO}_2^-]$ were also the highest (Fig. 11, a, b). Our

maximum $\Delta(15,18)$ was higher than the highest value of $\sim 2\text{‰}$ reported by Casciotti et al. (2013) for the same area, and could be explained by the extreme N-loss (and higher degree of NO_3^- isotopic fractionation) associated with the eddy.

3.3.1.3. Evidence from the $\Delta\delta^{15}\text{N}$ between NO_3^- and NO_2^-

$\Delta\delta^{15}\text{N}$ (see section 2.4.1) is also a good indicator for NO_2^- oxidation co-occurring with NO_3^- reduction. During NO_3^- reduction, the substrate is enriched in ^{15}N , and at steady state, the maximum difference between $\delta^{15}\text{N-NO}_3^-$ and $\delta^{15}\text{N-NO}_2^-$ should be the actual ϵ for NO_3^- reduction and thus no more than $\sim 20\text{-}30\text{‰}$ (Brandes et al., 1998; Voss et al., 2001; Granger et al., 2008). In the presence of NO_2^- reduction, though, $\Delta\delta^{15}\text{N}$ should be even lower (ϵ for NO_3^- reduction minus the ϵ for NO_2^- reduction at steady-state and in the absence of NO_2^- oxidation). As previously mentioned, NO_2^- oxidation is associated with an inverse kinetic ϵ which thereby increases $\Delta\delta^{15}\text{N}$. Accordingly, $\Delta\delta^{15}\text{N}$ values larger than the upper range for NO_3^- reduction alone (up to $\sim 40\text{‰}$ in the ETNP and ETSP) have been attributed to NO_2^- oxidation (Casciotti and McIlvin, 2007; Casciotti et al., 2013).

In this study, $\Delta\delta^{15}\text{N}$ was fairly constant around $35\text{-}40\text{‰}$ below 100-150 m depth through the OMZ, with a maximum value of up to $\sim 51\text{-}59\text{‰}$ at 200 m depth where the highest $\Delta(15,18)$ was also observed (Fig. 11, c, d). A large $\Delta\delta^{15}\text{N}$ could also be produced by NO_3^- reduction alone if the system was far from steady state. However, results from a time-dependent model by Casciotti et al. (2013) showed that $\Delta\delta^{15}\text{N}$ and $\delta^{15}\text{N-NO}_2^-$ distributions in O_2 depleted waters of the ETSP could not be reproduced in their model without NO_2^- oxidation, even in the heart of the OMZ. The highest values for $\Delta\delta^{15}\text{N}$ in this study occurred at the top of the OMZ ($\sigma_\theta = 26.2$, near the core of the eddy), where high rates of anammox have previously been measured from ^{15}N -labelled incubations (Lam et al., 2009). NO_2^- oxidation (coupled to CO_2 fixation) by anammox bacteria has a relatively larger inverse

kinetic ϵ (-31‰, Brunner et al., 2013) than aerobic (or microaerobic) nitrification ($\epsilon=-13$; Casciotti, 2009) and could explain, assuming steady-state, the larger $\Delta\delta^{15}\text{N}$ (and $\Delta(15,18)$) at this location.

Casciotti et al. (2013) found that the ratios of NO_2^- oxidation to NO_3^- and NO_2^- reduction increased with potential density (e.g. from 0 at $25.9 > \sigma_\theta < 26.3$ to up to 0.8 and 6.5, respectively, at $26.5 > \sigma_\theta < 26.8$) for both their steady-state and finite-difference (time-dependent) models in the OMZ of the ETSP. Comparison of our data to Casciotti et al. (2013) data for samples collected in the same region off Peru and their model results generally showed analogous distributions for $\delta^{15}\text{N-NO}_2^-$ and $\delta^{15}\text{N-NO}_3^-$ although our values were more extreme close to stations 162 (M90) and 87/88 (M91) because of the intense N-loss near the center of the eddy. This suggests similar NO_2^- oxidation patterns for this study. Higher ratios of NO_2^- oxidation to NO_3^- reduction at higher potential density (for the closed system model) could explain the higher $^{15}\epsilon_{\text{NO}_3^-/\text{red}}$ for deeper isopycnal ranges observed in this study (Table 1). Casciotti et al. (2013) also attributed the increase in $^{15}\epsilon_{\text{NO}_3^-/\text{red}}$ with potential density (from 14‰ to 22‰) to higher NO_2^- oxidation rates for the deepest isopycnal range in the same region.

4. Summary and concluding remarks

We observed intense N-loss (N_{def} of up to $\sim 44 \mu\text{mol L}^{-1}$) near the center of an anticyclonic mode-water eddy off the Peru Coast, confirming that eddies are N-loss hotspot in OMZ's. Near-coastal eddies likely transport and concentrate OM, a substrate for N-loss, offshore. More studies are still required to evaluate the impacts of this and similar transient features (e.g. eddies, current jets) on global N-loss.

$\delta^{15}\text{N}$ - and $\delta^{18}\text{O}$ of NO_3^- (up to ~ 70 ‰ and ~ 58 ‰) and $\delta^{15}\text{N-NO}_2^-$ (up to ~ 53 ‰) increased with substrate depletion in the OMZ as a consequence of isotopic fractionation during N-loss by denitrification or anammox. These isotope values are the highest ever

reported in marine environment. The $\delta^{15}\text{N-N}_2$ biogenic concurrently increased to up to $\sim 5\%$ at complete substrate consumption, which is also the average $\delta^{15}\text{N-NO}_3^-$ in the ocean.

We used this eddy, which has intense N-loss and simplified hydrography, as a natural experiment to better constrain the environmental ϵ values for NO_3^- reduction ($^{15}\epsilon_{\text{NO}_3^- \text{ red}}$) and net N-loss in the OMZ of the ETSP. We compared different approaches to calculate ϵ , i.e. 1) closed versus open systems, 2) assuming Redfield stoichiometry versus using $[\text{N}_2]_{\text{biogenic}}$ data to estimate the initial substrate concentration, and 3) calculating ϵ for net N-loss from the $\delta^{15}\text{N}$ of the substrate ($\text{NO}_3^- + \text{NO}_2^-$, $^{15}\epsilon_{\text{DIN-loss}}$) versus the $\delta^{15}\text{N}$ of the product (biogenic N_2 , $\epsilon_{\square\text{N}_2}$). $^{15}\epsilon_{\text{NO}_3^- \text{ red}}$ varied from 12% to up to 31% for a closed system and was generally higher for deeper isopycnals, where NO_2^- oxidation to NO_3^- reduction is likely to be higher, according to Casciotti et al. (2013). No significant difference was observed for ϵ calculated assuming Redfield stoichiometry or using $[\text{N}_2]_{\text{biogenic}}$ data to calculate N_{exp} , suggesting that both approaches are valid, at least in the OMZ of the ETSP. These results, together with further insights from the decoupling of N and O of NO_3^- isotopes ($\Delta(15,18)$) and the difference between $\delta^{15}\text{N-NO}_3^-$ and $\delta^{15}\text{N-NO}_2^-$ ($\Delta\delta^{15}\text{N}$), confirm that NO_2^- oxidation can increase the ϵ associated with NO_3^- reduction. Therefore, previous studies likely over-estimated $\epsilon_{\text{NO}_3^- \text{ red}}$ (e.g. see Brandes et al., 1998; Voss et al., 2001) in regions where NO_2^- accumulates.

We obtained a low overall ϵ for net N-loss ($^{15}\epsilon_{\text{DIN-loss}}$ and ϵ_{bN_2}) of $\sim 13\text{-}14\%$ for a closed system and $16\text{-}19\%$ for an open system. It follows that reliable measurements for $\delta^{15}\text{N-N}_2$ are a powerful tool for oceanographers to directly estimate ϵ of N-loss in OMZs given the influences of processes such as NO_2^- oxidation on ϵ estimated from NO_3^- isotopic composition alone. The observed low $^{15}\epsilon_{\text{DIN-loss}}$ and $\epsilon_{\square\text{N}_2}$ compared to canonical values of $20\text{-}30\%$ assumed for marine environments (Brandes et al., 1998; Voss et al., 2001; Granger et al.,

2008), implies a global ocean N budget closer to balance if this value is common for OMZ N-loss.

Acknowledgements

Data for this paper are available on the Data Management Portal for Kiel Marine Sciences hosted at GEOMAR (M90 and M91 cruises): <https://portal.geomar.de/>. This work was supported by the Deutsche Forschungsgemeinschaft- project SFB-754 (www.sfb754.de), SOPRANII (grant # FKZ03F0611A; www.sopran.pangaea.de) and a NSERC Postdoctoral Fellowship to A.B. We would like to thank the captain and crew of R/V Meteor during the M90 and M91 cruises and Martin Frank, Tina Baustian, Martina Lohmann, Janett Voigt, Kristin Doering, Patrick Daniel, Daniel Kiefhaber, Avi Bernales and Violeta Leon for their help during sampling and/or sample analysis. We thank the authorities of Peru for the permission to work in their territorial waters.

References

- Alkhatib M., M. F. Lehmann, and P. A. del Giorgio (2012), The nitrogen isotope effect of benthic remineralization-nitrification-denitrification coupling in an estuarine environment, *Biogeosciences*, 9, 1633–1646.
- Altabet M. A. (2001), Nitrogen isotopic evidence for micronutrient control of fractional NO_3^- utilization in the equatorial Pacific, *Limnol. Oceanogr.*, 46(2), 368–380.
- Altabet M. A. (2005) Isotopic tracers of the marine nitrogen cycle: present and past, in *The handbook of environmental chemistry*, vol. 2, edited by O. Hutzinger, pp. 251–293, Springer-Verlag, Berlin, Heidelberg.
- Altabet M. A. (2007), Constraints on oceanic N balance/imbalance from sedimentary ^{15}N records, *Biogeosciences*, 4, 75–86.
- Altabet M. A., E. Ryabenko, L. Stramma, D. W. R. Wallace, M. Frank, P. Grasse and G. Lavik (2012), An eddy-stimulated hotspot for fixed nitrogen-loss from the Peru oxygen minimum zone, *Biogeosciences*, 9, 4897–4908.
- Babbin A. R., R. G. Keil, A. H. Devol and B. B. Ward (2014), Organic matter stoichiometry, flux, and oxygen control nitrogen loss in the Ocean, *Science*, 344, 406–408.
- Bourbonnais A., M. F. Lehmann, J. J. Waniek and D. E. Schulz-Bull (2009), Nitrate isotope anomalies reflect N_2 fixation in the Azores Front region (subtropical NE Atlantic), *J. Geophys. Res.*, 114, C03003, doi:10.1029–2007JC004617.

- Bourbonnais A., M. F. Lehmann, R. C. Hamme, C. C. Manning and S. K. Juniper (2013), Nitrate elimination and regeneration as evidenced by dissolved inorganic nitrogen isotopes in Saanich Inlet, a seasonally anoxic fjord, *Mar. Chem.*, 157, 194–207.
- Brandes J. A. and A. H. Devol (2002), A global marine-fixed nitrogen isotopic budget: Implications for Holocene nitrogen cycling. *Global Biogeochem. Cycles*, 16(4), 67:1–14.
- Brandes J. A., A. H. Devol, T. Yoshinari, D. A. Jayakumar and S. W. A. Naqvi (1998), Isotopic composition of nitrate in the central Arabian Sea and eastern tropical North Pacific: A tracer for mixing and nitrogen cycles. *Limnol. Oceanogr.*, 43(7), 1680–1689.
- Brunner B., S. Contreras, M. F. Lehmann, O. Matantseva, M. Rollog, T. Kalvelage, G. Klockgether, G. Lavik, M. S. M. Jetten, B. Kartal and M. M. M. Kuypers (2013), Nitrogen isotope effects induced by anammox bacteria, *PNAS*, 110(47), 18994–18999.
- Bryan B. A., G. Shearer, J. L. Skeeters and D. H. Kohl (1983), Variable expression of the nitrogen isotope effect associated with denitrification of nitrite, *J. Biol. Chem.*, 258(14), 8613–8617.
- Buchwald C. and K. L. Casciotti (2010), Oxygen isotopic fractionation and exchange during bacterial nitrite oxidation, *Limnol. Oceanogr.*, 55(3), 1064–1074.
- Canfield D. E., F. J. Stewart, B. Thamdrup, L. De Brabandere, T. Dalsgaard, E. F. Delong, N. P. Revsbech and O. Ulloa (2010), A cryptic sulfur cycle in oxygen-minimum zone waters off the Chilean coast, *Science*, 330(6009), 1375–1378.
- Casciotti, K. L. (2009), Inverse kinetic isotope fractionation during bacterial nitrite oxidation. *Geochim. Cosmochim. Ac.*, 73, 2061–2076.
- Casciotti, K. L. and C. Buchwald (2012), Insights on the marine microbial nitrogen cycle from isotopic approaches to nitrification, *Frontiers in Microbiology*, 3(356), 1–14, doi: 10.3389/fmicb.2012.00356
- Casciotti K. L. and M. R. McIlvin (2007), Isotopic analyses of nitrate and nitrite from reference mixtures and application to Eastern Tropical North Pacific waters, *Mar. Chem.*, 107, 184–201.
- Casciotti K. L., J. K. Böhlke, M. R. McIlvin, S. J. Mroczkowski and J. E. Hannon (2007) Oxygen Isotopes in Nitrite: Analysis, Calibration, and Equilibration. *Anal. Chem.*, 79, 2427–2436.
- Casciotti K. L., C. Buchwald and M. McIlvin (2013), Implications of nitrate and nitrite isotopic measurements for the mechanisms of nitrogen cycling in the Peru oxygen deficient zone, *Deep-Sea Res. PT I*, 80, 78–93.
- Chaigneau A., A. Gizolme and C. Grados (2008), Mesoscale eddies off Peru in altimeter records: identification algorithms and eddy spatio-temporal patterns, *Prog. Oceanogr.*, 79, 106–119.
- Chaigneau A., G. Eldin and B. Dewitte (2009), Eddy activity in the four major upwelling systems from satellite altimetry (1992–2007), *Prog. Oceanogr.*, 83, 117–123.

- Chang B. X., A. H. Devol and S. R. Emerson (2010), Denitrification and the nitrogen gas excess in the eastern tropical South Pacific oxygen deficient zone, *Deep-Sea Res. PT I*, 57, 1092–1101.
- Chang B. X., A. H. Devol and S. R. Emerson (2012), Fixed nitrogen loss from the eastern tropical North Pacific and Arabian Sea oxygen deficient zones determined from measurements of N₂:Ar. *Global Biogeochem. Cycles*, 26, GB3030, doi:10.1029/2011GB004207.
- Charoenpong C. N., L. A. Bristow and M. A. Altabet (2014), A continuous flow isotope ratio mass spectrometry method for high precision determination of dissolved gas ratios and isotopic composition, *Limnol. Oceanogr.: Methods*, 12, 323–337.
- Chelton D. B., M. G. Schlax and R. M. Samelson (2011), Global observations of nonlinear mesoscale eddies, *91*(2), 167–216.
- Codispoti L. A. (2007), An oceanic fixed nitrogen sink exceeding 400 Tg N a⁻¹, *Biogeosciences*, 4, 233–253.
- Dähnke, k. and B. Thamdrup (2013), Nitrogen isotope dynamics and fractionation during sedimentary denitrification in Boknis Eck, Baltic Sea, *Biogeosciences*, 10, 3079–3088.
- Deutsch, C., D. M. Sigman, R. C. Thunell, A. N. Meckler, and G. H. Haug (2004), Isotopic constraints on glacial/interglacial changes in the oceanic nitrogen budget, *Global Biogeochem. Cycles*, 18, GB4012, doi:10.1029/2003GB002189.
- Devol A. H., A. G. Uhlenhopp, S. W. A. Naqvi, J. A. Brandes, D. A. Jayakumar, H. Naik, S. Gaurin, L. A. Codispoti and T. Yoshinari (2006), Denitrification rates and excess nitrogen gas concentrations in the Arabian Sea oxygen deficient zone, *Deep Sea Res. PT I*, 53, 1533–1547.
- DeVries T., C. Deutsch, P. A. Rafter, F. Primeau (2013), Marine denitrification rates determined from a global 3-D inverse model, *Biogeosciences*, 10, 2481–2496.
- Frey C., J. W. Dippner, and M. Voss (2014), Close coupling of N-cycling processes expressed in stable isotope data at the redoxcline of the Baltic Sea, *Global Biogeochem. Cycles*, 28(9), 974–991.
- Füssel J., P. Lam, G. Lavik, M. M. Jensen, M. Holtappels, M. G. Gunter and M. M. M. Kuypers (2011), Nitrite oxidation in the Namibian oxygen minimum zone, *ISME J.*, 6, 1200–1209.
- Granger J., and D. M. Sigman (2009), Removal of nitrite with sulfamic acid for nitrate N and O isotope analysis with the denitrifier method, *Rapid Commun. Mass Spectrom.*, 23(23), 3753–3762.
- Granger J., D. M. Sigman, J. A. Needoba and P. J. Harrison (2004), Coupled nitrogen and oxygen isotope fractionation of nitrate during assimilation by cultures of marine phytoplankton, *Limnol. Oceanogr.*, 49(5), 1763–1773.
- Granger J., D. M. Sigman, M. F. Lehmann and P. D. Tortell (2008), Nitrogen and oxygen isotope fractionation during dissimilatory nitrate reduction by denitrifying bacteria,

Limnol. Oceanogr., 53(6), 2533–2545.

Großkopt, T., W. Mohr, T. Baustian, H. Schunck, D. Gill, M. M. M. Kuypers, G. Lavik, R. A. Schmitz, D. W. R. Wallace, and J. Laroche (2012), Doubling of marine dinitrogen-fixation rates based on direct measurements, *Nature*, 488, 361–364.

Gruber N. (2004), The dynamics of the marine nitrogen cycle and its influence on atmospheric CO₂ variations, in: *The Ocean Carbon Cycle and Climate*, edited by M. Follows and T. Oguz, pp. 97–148, Kluwer Acad., Dordrecht, The Netherlands.

Gruber N. (2008), The Marine Nitrogen Cycle: Overview and Challenges, in: *Nitrogen in the marine environment*, edited by D. G. Capone, D. A. Bronk, M. R. Mulholland and E. J. Carpenter, pp. 1–50, Elsevier, Amsterdam, The Netherlands.

Hamme R. C. and S. R. Emerson (2002), Mechanisms controlling the global oceanic distribution of the inert gases argon, nitrogen and neon, *Geophys. Res. Lett.*, 29(23), 2120.

Kalvelage T., G. Lavik, P. Lam, S. Contreras, L. Arteaga, C. R. Löscher, A. Oschlies, A. Paulmier, L. Stramma and M. M. M. Kuypers (2013), Nitrogen cycling driven by organic matter export in the South Pacific oxygen minimum zone, *Nat. Geosci.*, 6, 228–234.

Keeling R. F. and H. E. Garcia (2002), The change in oceanic O₂ inventory associated with recent global warming, *PNAS*, 99, 7848–7853.

Kunze E., R. W. Schmitt, and J. M. Toole (1995), The energy balance in a warm-core ring's near-inertial critical layer, *J. Phys. Oceanogr.*, 25, 942–957.

Kritee K., D. M. Sigman, J. Granger, B. B. Ward, A. Jayakumar and C. Deutsch (2012) Reduced isotope fractionation by denitrification under conditions relevant to the ocean. *Geochim. Cosmochim. Ac.*, 92, 243–259.

Lam P., G. Lavik, M. M. Jensen, J. van de Vossenberg, M. Schmid, D. Woebken, D. Gutierrez, R. Amann, M. S. M. Jetten and M. M. M. Kuypers (2009), Revising the nitrogen cycle in the Peruvian oxygen minimum zone, *PNAS*, 106, 4752–4757.

Lam P. and M. M. M. Kuypers (2011), Microbial Nitrogen Cycling Processes in Oxygen Minimum Zones, *Annu. Rev. Marine. Sci.*, 3, 317–345.

Lehmann M. F., D. M. Sigman, D. C. McCorkle, B. G. Brunelle, S. Hoffmann, M. Kienast, G. Cane and J. Clement (2005), Origin of the deep Bering Sea nitrate deficit: Constraints from the nitrogen and oxygen isotopic composition of water column nitrate and benthic nitrate fluxes, *Global Biogeochem. Cycles*, 19, GB4005–doi:10.1029–2005GB002508.

Lehmann M. F., D. M. Sigman, D. C. McCorkle, J. Granger, S. Hoffmann, G. Cane and B. G. Brunelle (2007), The distribution of nitrate ¹⁵N/¹⁴N in marine sediments and the impact of benthic nitrogen loss on the isotopic composition of oceanic nitrate, *Geochim. Cosmochim. Ac.*, 71, 5384–5404.

Mariotti A., J. C. Germon, P. Hubert, P. Kaiser, R. Letolle, A. Tardieux and P. Tardieux (1981), Experimental determination of nitrogen kinetic isotope fractionation: Some principles; illustration for the denitrification and nitrification processes, *Plant Soil*, 62,

- McGillicuddy D. J. Jr, L. A. Anderson, N. R. Bates, T. Bibby, K. O. Buesseler, C. A. Carlson, C. S. Davis, C. Ewart, P. G. Falkowski, S. A. Goldthwait, D. A. Hansell, W. J. Jenkins, R. Johnson, V. K. Kosnyrev, J. R. Ledwell, Q. P. Li, D. A. Siegel and D. K. Steinberg (2007), Eddy/Wind Interactions Stimulate Extraordinary Mid-Ocean Plankton Blooms, *Science*, 316, 1021–1026.
- McIlvin M. R. and Altabet M. A. (2005), Chemical Conversion of Nitrate and Nitrite to Nitrous Oxide for Nitrogen and Oxygen Isotopic Analysis in Freshwater and Seawater, *Anal. Chem.*, 77, 5589–5595.
- Reed D. C., Slomp C. P. and Gustafsson B. G. (2011), Sedimentary phosphorus dynamics and the evolution of bottom-water hypoxia: A coupled benthic-pelagic model of a coastal system, *Limnol. Oceanogr.: Methods*, 56, 1075–1092.
- Sigman D. M., R. Robinson, A. N. Knapp, A. van Geen, D. C. McCorkle, J. A. Brandes and R. C. Thunell (2003), Distinguishing between water column and sedimentary denitrification in the Santa Barbara Basin using the stable isotopes of nitrate, *Geochem. Geophys. Geosyst.*, 4, 1040, doi:10.1029/2002GC000384.
- Sigman D. M., J. Granger, P. J. DiFiore, M. F. Lehmann, R. Ho, G. Cane and A. van Geen (2005), Coupled nitrogen and oxygen isotope measurements of nitrate along the eastern North Pacific margin, *Global Biogeochem. Cycles*, 19, GB4022–doi:10.1029/2005GB002458.
- Sigman D. M., P. J. DiFiore, M. P. Hain, C. Deutsch, Y. Wang, D. M. Karl, A. N. Knapp, M. F. Lehmann and S. Pantoja (2009), The dual isotopes of deep nitrate as a constraint on the cycle and budget of oceanic fixed nitrogen, *Deep-Sea Res. PT I*, 56, 1419–1439.
- Stramma L., S. Schmidtko, L. A. Levin and G. C. Johnson (2010), Ocean oxygen minima expansions and their biological impacts, *Deep-Sea Res. PT I*, 57, 587–595.
- Stramma L., H. W. Bange, R. Czeschel, A. Lorenzo and M. Frank (2013), On the role of mesoscale eddies for the biological productivity and biogeochemistry in the eastern tropical Pacific Ocean off Peru, *Biogeosciences*, 10, 7293–7306.
- Voss M., J. W. Dippner and J. Montoya (2001), Nitrogen isotope patterns in the oxygen-deficient waters of the Eastern Tropical North Pacific Ocean, *Deep-sea Res. PT I*, 48, 1905–1921.
- Wada E. and A. Hattori (1976), Natural abundance of ^{15}N in particulate organic matter in the North Pacific Ocean, *Geochim. Cosmochim. Ac.*, 40, 249–251.
- Wallmann K. (2010), Phosphorus imbalance in the global ocean? *Global Biogeochem. Cycles*, 24, GB4030, doi:10.1029/2009GB003643.
- Ward B. B., A. H. Devol, J. J. Rich, A. Chaigneau, S. E. Bulow, H. Naik, A. Pratihary and A. Jayakumar (2009), Denitrification as the dominant nitrogen loss process in the Arabian Sea, *Nature*, 461, 78–81.
- Wenk, C. B., J. Zopfi, J. Blees, M. Veronesi, H. Niemann, M. F. Lehmann (2014),

Community N and O isotope fractionation by sulfide-dependent denitrification and anammox in a stratified lacustrine water column, 125, 551–563.

Accepted Article

Table 1. Isotope effects for NO_3^- reduction ($^{15}\epsilon_{\text{NO}_3^- \text{red}}$), and net N-loss calculated using both the substrate (NO_3^- and NO_2^- ; eq. 9, $^{15}\epsilon_{\text{DIN-loss}}$) and the product (biogenic N_2 ; eq. 10, ϵ_{bN_2}) for a closed system as well as average $[\text{NO}_3^-]$ and $[\text{NO}_2^-]$ (and their ranges in brackets) for different isopycnal ranges during the M90 (Nov. 2012) and M91 (Dec. 2012) cruises. Results from calculations based on the sum of N pools (i.e. substrates (NO_3^- , NO_2^-) and product (biogenic N_2) of N-loss processes) or Redfield stoichiometry to calculate N_{exp} and ϵ are shown. The standard errors of the slope and intercept, which respectively represent ϵ and the initial $\delta^{15}\text{N-NO}_3^-$ or $\delta^{15}\text{N-DIN}$, are indicated.

Isopycnal (kg L^{-1})	$^{15}\epsilon$ (‰)	Intercept	r^2	n	$^{15}\epsilon$ (‰)	Intercept	r^2	n	$[\text{NO}_3^-]$ ($\mu\text{mol L}^{-1}$)	$[\text{NO}_2^-]$ ($\mu\text{mol L}^{-1}$)	
M90	Based on sum of N pools				Based on Redfield stoichiometry						
$\delta^{15}\text{N-NO}_3^-$ ^a											
>26.2-≤26.3	12.0 ± 2.8	15.9 ± 7.7	0.86	5	12.7 ± 2.3	11.5 ± 6.0	0.89	6	7.9 ± 7.4 (0.3-19.5)	6.1 ± 3.7 (0.02-10.9)	
>26.3-≤26.4	23.0 ± 2.9	2.0 ± 3.6	0.95	5	20.8 ± 1.7	3.6 ± 2.2	0.97	6	11.9 ± 3.1 (6.2-14.0)	7.2 ± 1.8 (4.7 ± 10.0)	
>26.4-≤26.5	24.1 ± 1.8	4.6 ± 1.5	0.97	8	22.8 ± 2.1	5.1 ± 1.8	0.95	8	16.9 ± 4.0 (10.5-21.5)	6.0 ± 3.2 (0.01-9.8)	
>26.5-≤26.6	30.9 ± 2.3	2.4 ± 1.4	0.96	10	28.5 ± 1.3	3.7 ± 0.8	0.98	10	21.7 ± 2.8 (17.6-27.4)	5.7 ± 2.5 (0.01-8.0)	
>26.6-≤26.7	29.0 ± 7.1	4.5 ± 2.2	0.77	7	32.0 ± 3.0	3.9 ± 0.9	0.96	7	29.6 ± 2.5 (25.9-33.1)	2.0 ± 1.6 (0.01-4.1)	
>26.7-≤26.8	29.0 ± 6.3	4.4 ± 4.4	0.88	5	28.3 ± 1.9	5.3 ± 0.3	0.98	7	34.4 ± 2.6 (29.4-36.7)	0.8 ± 1.3 (0.01-3.5)	
>26.3	20.9 ± 0.7	6.8 ± 0.5	0.96	41	19.4 ± 0.6	7.5 ± 0.4	0.96	44	25.2 ± 9.6 (6.2-40.7)	3.8 ± 3.3 (0.01-10.0)	
$\delta^{15}\text{N-DIN}$ ^a											
>26.2-≤26.3	4.5 ± 1.1	12.8 ± 1.1	0.86	5	4.5 ± 0.7	12.2 ± 0.8	0.91	6			
>26.3-≤26.4	9.5 ± 4.1	9.1 ± 2.8	0.64	5	9.1 ± 1.3	8.7 ± 1.0	0.90	7			
>26.4-≤26.5	17.5 ± 2.1	5.9 ± 1.0	0.93	7	14.9 ± 2.5	6.8 ± 1.3	0.73	7			
>26.5-≤26.6	15.3 ± 5.3	7.3 ± 1.8	0.51	9	18.3 ± 3.5	6.2 ± 1.2	0.77	10			
>26.6-≤26.7	13.4 ± 6.5	7.3 ± 1.6	0.51	6	13.3 ± 2.9	7.6 ± 0.7	0.84	6			
>26.7-≤26.8	na	na	na	na	15.6 ± 3.1	6.9 ± 0.4	0.84	7			
>26.3	13.2 ± 0.6	7.5 ± 0.2	0.92	40	11.6 ± 0.5	7.9 ± 0.2	0.93	43			
$\delta^{15}\text{N-biogenic N}_2$ ^b											
26.0-26.5	14.3 ± 1.3	6.3 ± 0.7	0.89	18	14.4 ± 1.2	5.9 ± 0.7	0.90	18			
M91	Based on sum of N pools				Based on Redfield stoichiometry						
$\delta^{15}\text{N-NO}_3^-$ ^a											
>26.2-≤26.3	23.3 ± 2.2	5.6 ± 4.6	0.98	5	23.4 ± 2.6	12.0 ± 6.0	0.95	6	4.2 ± 4.0 (0.2-12.1)	7.6 ± 2.1 (3.6-11.0)	
>26.3-≤26.4	18.7 ± 1.3	6.0 ± 2.0	0.98	6	16.4 ± 1.4	6.6 ± 2.1	0.95	9	11.2 ± 4.4 (3.7-16.5)	7.5 ± 2.1 (4.6-10.7)	
>26.4-≤26.5	22.4 ± 1.2	6.3 ± 1.1	0.99	6	17.9 ± 2.5	7.8 ± 2.6	0.88	9	16.3 ± 3.9 (9.2-22.7)	7.3 ± 2.3 (4.2-10.8)	
>26.5-≤26.7	25.6 ± 3.8	4.6 ± 2.1	0.92	6	na	na	na	na	25.8 ± 6.3 (19.0-38.9)	5.1 ± 2.2 (1.3-7.6)	
>26.7-≤26.9	14.9 ± 8.5	6.7 ± 1.5	0.51	5	10.0 ± 3.9	6.7 ± 1.0	0.61	6	37.3 ± 3.8 (32.0-42.9)	0.4 ± 0.7 (0.01-1.8)	
>26.3	19.5 ± 1.1	7.3 ± 1.0	0.92	28	17.6 ± 1.0	6.9 ± 0.9	0.91	37	23.9 ± 11.5 (3.7-42.9)	4.5 ± 3.6 (0.01-10.8)	

$\delta^{15}\text{N-DIN}^a$								
>26.2-≤26.3	6.5 ± 3.1	10.0 ± 3.2	0.52	6	7.1 ± 2.7	8.7 ± 3.0	0.63	6
>26.3-≤26.4	na	na	na	na	na	na	na	na
>26.4-≤26.5	16.1 ± 5.2	6.2 ± 2.6	0.70	6	11.7 ± 4.5	7.7 ± 2.5	0.53	8
>26.5-≤26.7	13.4 ± 5.1	7.2 ± 1.7	0.63	6	12.0 ± 5.5	7.4 ± 1.8	0.49	7
>26.7-≤26.9	na	na	na	na	na	na	na	na
>26.3	12.6 ± 0.9	7.1 ± 0.5	0.89	27	8.3 ± 1.3	9.3 ± 0.7	0.57	31
$\delta^{15}\text{N-biogenic N}_2^b$								
26.0-26.5	14.2 ± 2.2	7.1 ± 1.3	0.62	27	14.8 ± 2.1	7.0 ± 1.2	0.66	27

^a Only data with $[\text{O}_2] < 10 \mu\text{mol L}^{-1}$ and deeper than 100 m were considered.

^b Only data with $\geq 7.5 \mu\text{mol L}^{-1}$ biogenic N_2 were considered.

Accepted Article

Table 2. Isotope effects for NO_3^- reduction ($^{15}\epsilon_{\text{NO}_3^- \text{red}}$), and net N loss calculated using both the substrate (NO_3^- and NO_2^- ; eq. 11, $^{15}\epsilon_{\text{DIN-loss}}$) and the product (biogenic N_2 ; eq. 12, ϵ_{bN_2}) for an open system during the M90 (Nov. 2012) and M91 (Dec. 2012) cruises. The standard errors of the slope and intercept are indicated.

Isopycnal ranges (kg L^{-1})	$^{15}\epsilon$	Intercept	r^2	n
M90				
$\delta^{15}\text{N-NO}_3^-$ ^a				
>26.2-≤26.3	127.9 ± 22.8	-62.8 ± 19.5	0.91	5
>26.3-≤26.4	87.9 ± 14.0	-30.6 ± 9.6	0.93	5
>26.4-≤26.5	55.8 ± 4.6	-6.2 ± 2.5	0.96	8
>26.5-≤26.6	53.8 ± 3.1	-3.1 ± 1.4	0.97	10
>26.6-≤26.7	38.2 ± 9.6	3.3 ± 2.6	0.76	7
>26.7-≤26.8	35.7 ± 7.4	3.8 ± 1.4	0.89	5
>26.3	38.8 ± 1.6	3.4 ± 0.7	0.94	41
$\delta^{15}\text{N-DIN}$ ^a				
>26.2-≤26.3	13.3 ± 2.3	9.1 ± 1.5	0.91	5
>26.3-≤26.4	18.4 ± 7.9	6.5 ± 3.8	0.65	5
>26.4-≤26.5	26.7 ± 3.4	4.2 ± 1.3	0.94	7
>26.5-≤26.6	22.7 ± 7.5	6.0 ± 2.2	0.53	10
>26.6->26.7	22.7 ± 7.3	5.7 ± 1.6	0.71	6
≤26.8	na	na	na	na
>26.3	19.3 ± 0.8	6.7 ± 0.2	0.94	40
$\delta^{15}\text{N-biogenic N}_2$ ^b				
26.0-26.5	17.3 ± 1.3	4.9 ± 0.5	0.91	18
M91				
$\delta^{15}\text{N-NO}_3^-$ ^a				
>26.2-≤26.3	161.0 ± 32.8	-92.6 ± 27.7	0.89	5
>26.3-≤26.4	78.4 ± 13.5	-25.5 ± 10.1	0.87	6
>26.4-≤26.5	60.8 ± 3.2	-9.0 ± 1.9	0.99	6
>26.5-≤26.7	43.2 ± 6.1	0.8 ± 2.6	0.93	6
>26.7-≤26.9	16.5 ± 10.3	6.7 ± 1.6	0.46	5
>26.3	41.7 ± 2.6	2.8 ± 1.3	0.91	28
$\delta^{15}\text{N-DIN}$ ^a				
>26.1-≤26.3	17.7 ± 8.0	5.4 ± 5.1	0.55	6
>26.3-≤26.4	na	na	na	na
>26.4-≤26.5	27.6 ± 8.1	3.4 ± 3.1	0.74	6
>26.5-≤26.7	17.9 ± 6.6	6.6 ± 1.9	0.65	6
>26.7-≤26.9	na	na	na	na
>26.3	19.1 ± 1.1	6.1 ± 0.4	0.92	27
$\delta^{15}\text{N-biogenic N}_2$ ^b				
26.0-26.5	15.7 ± 2.5	5.1 ± 1.0	0.78	28

^a Only data with $[\text{O}_2] < 10 \mu\text{mol L}^{-1}$ and deeper than 100 m were considered.

^b Only data with $\geq 7.5 \mu\text{mol L}^{-1}$ biogenic N_2 were considered

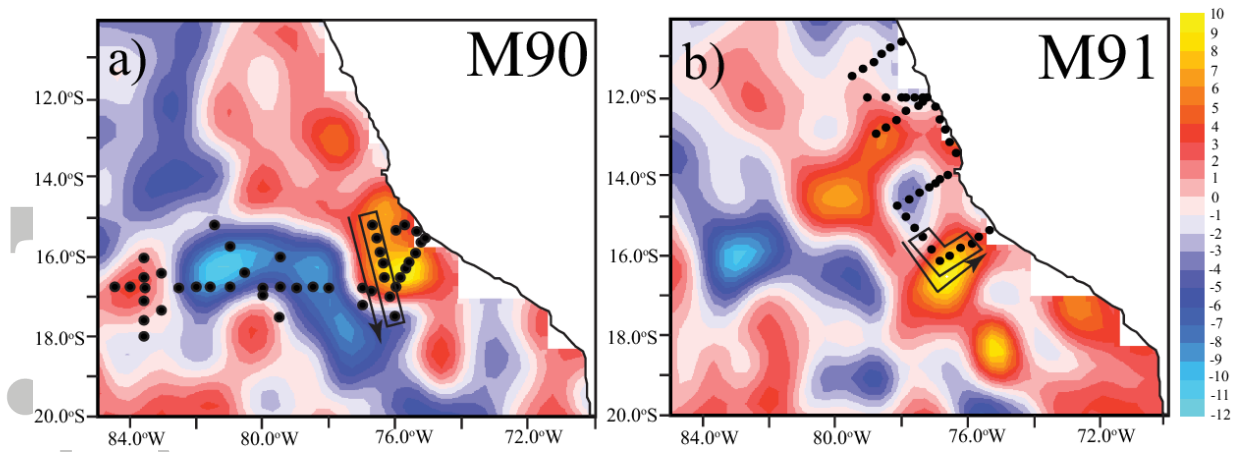


Figure 1. Maps showing stations sampled (black dots) during the M90 (a) and M91 (b) cruises. Contours indicate the delayed time, 7-day, mean SSHA (in cm) for 21 November 2012 (a) and 19 December 2012 (b). The transects of Eddy A (black rectangles) used for our analysis are shown. SSHA data are from Aviso (<http://www.aviso.oceanobs.com>).

Accepted Article

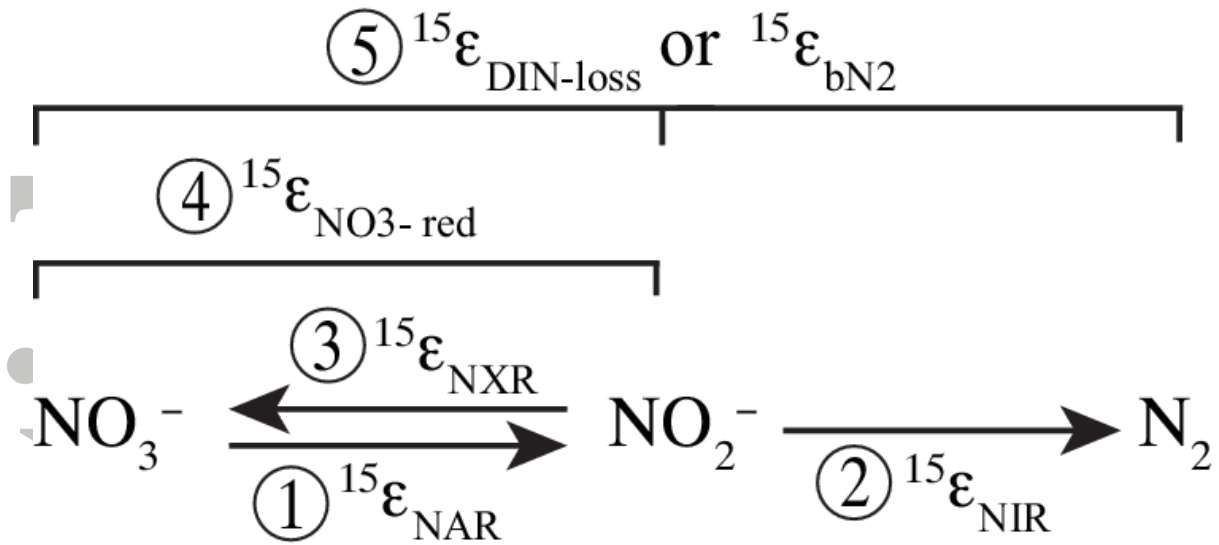


Figure 2. Terminology used for the different ϵ 's derived in this study. $^{15}\epsilon_{\text{NAR}}$ is the ϵ associated with the NO_3^- reduction to NO_2^- (1), $^{15}\epsilon_{\text{NIR}}$ is the ϵ associated with NO_2^- reduction to biogenic N_2 (2), $^{15}\epsilon_{\text{NXR}}$ is the isotope effect associated with NO_2^- oxidation to NO_3^- (3), $^{15}\epsilon_{\text{NO}_3\text{-red}}$ is the net observed ϵ associated with NO_3^- reduction, which is also influenced by NO_2^- oxidation (4), and $^{15}\epsilon_{\text{DIN-loss}}$ and $^{15}\epsilon_{\text{bN}_2}$ (see section 3.2.3) are the net ϵ associated with overall N-loss (5), and influenced by all processes (1 to 3).

Accepted

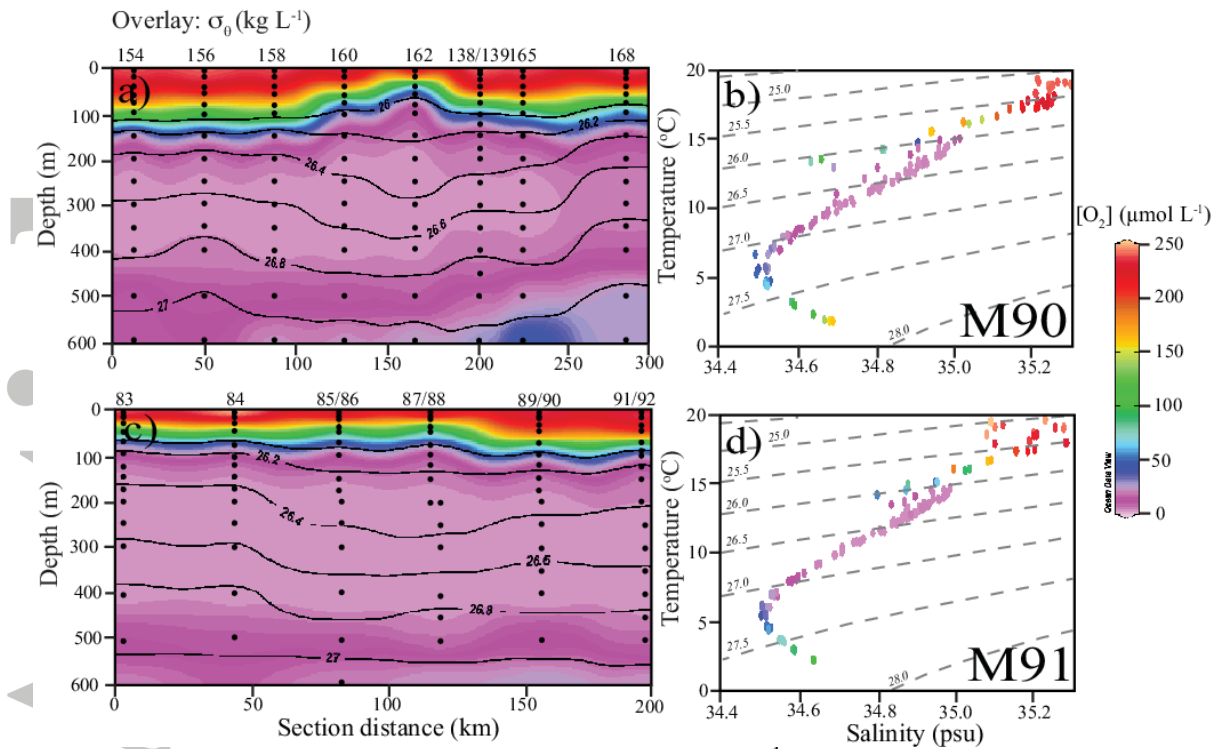


Figure 3. Section plots of Eddy A showing [O₂] ($\mu\text{mol L}^{-1}$) and temperature versus salinity for transects made during the M90 (a, b) and M91 cruises (c, d). σ_θ (kg L^{-1}) contours are shown in overlay in a and c. Black dots represent sampled depths for each station. Station numbers are indicated above plots a and c.

Accepted

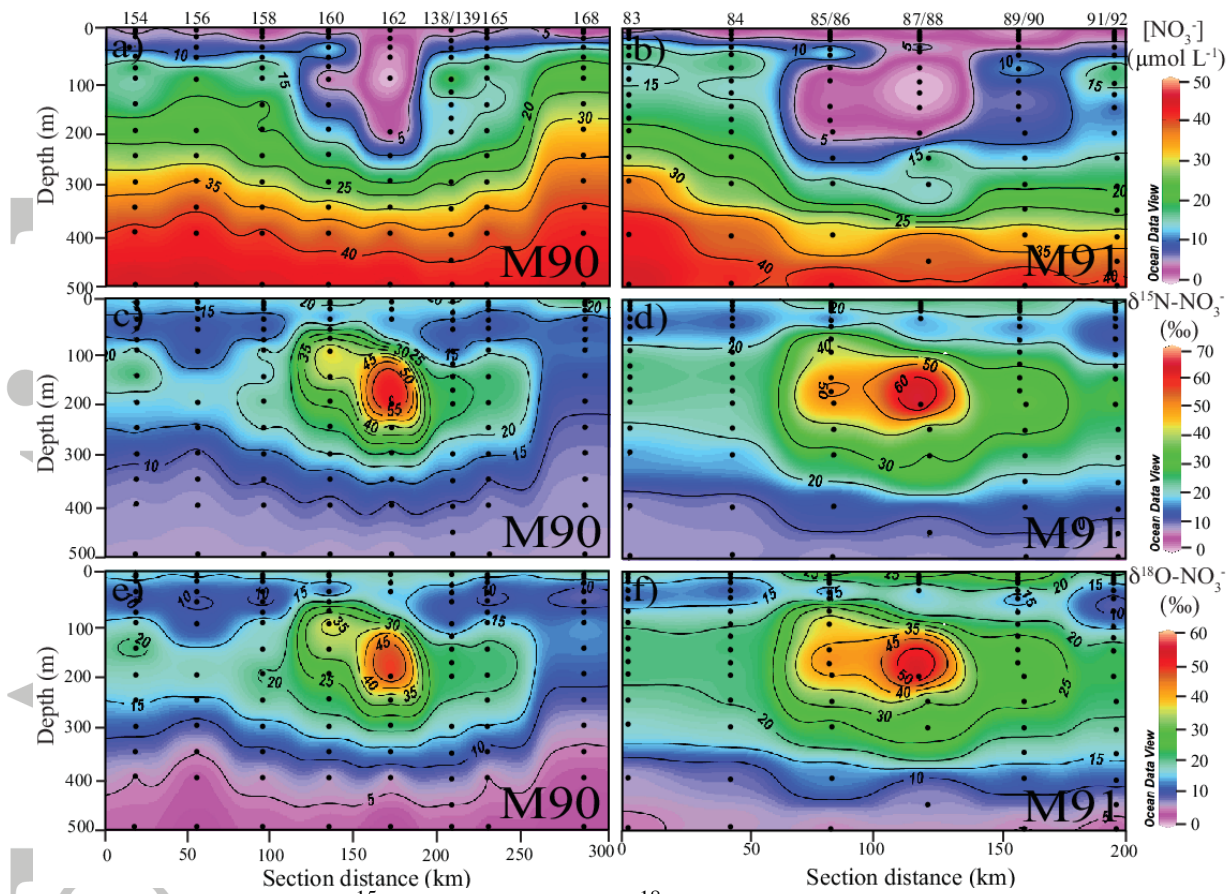


Figure 4. $[\text{NO}_3^-]$ (a, b), $\delta^{15}\text{N-NO}_3^-$ (c, d), and $\delta^{18}\text{O-NO}_3^-$ (e, f) for transects made during the M90 (a, c, e) and M91 (b, d, f) cruises (see Fig. 1).

Accepte

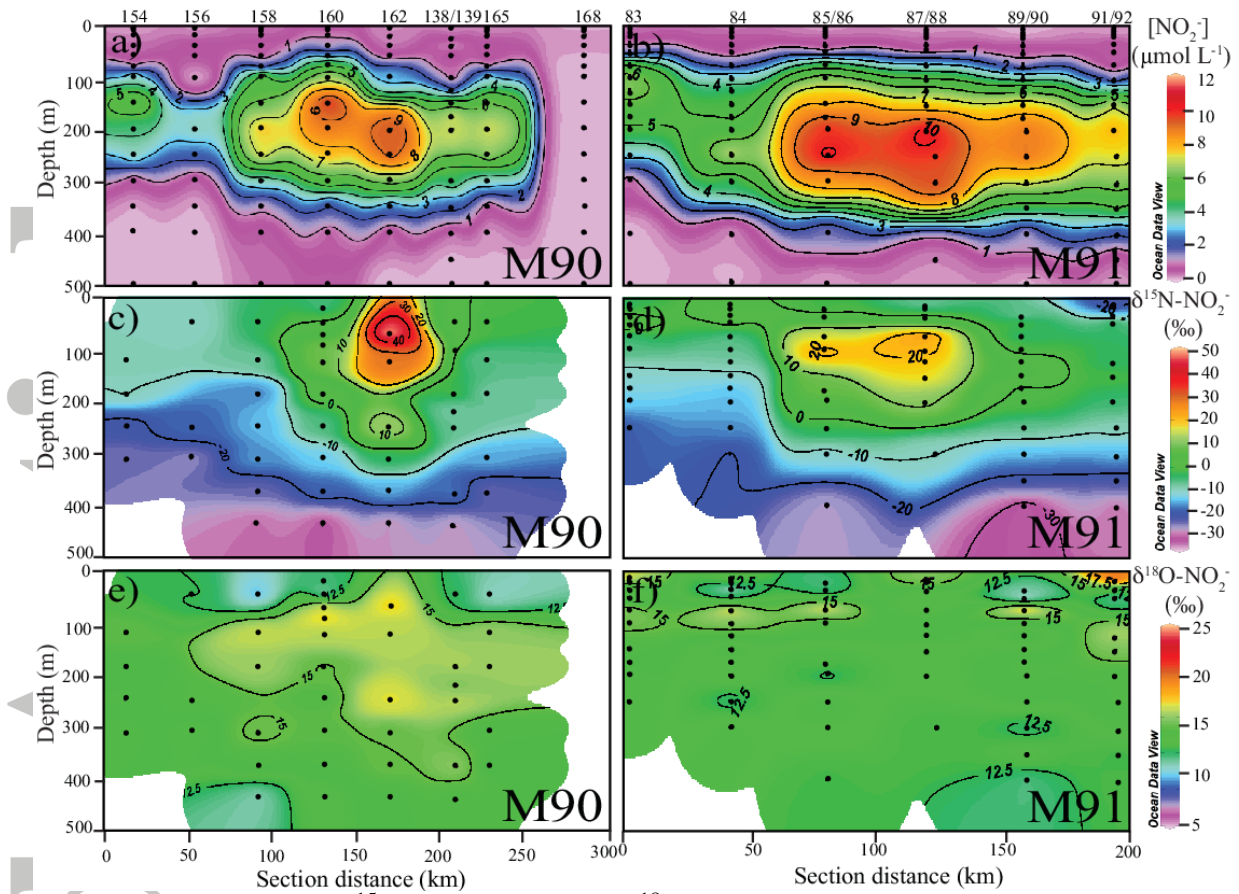


Figure 5. $[NO_2^-]$ (a, b), $\delta^{15}\text{N-NO}_2^-$ (c, d), and $\delta^{18}\text{O-NO}_2^-$ (e, f) for transects made during the M90 (a, c, e) and M91 (b, d, f) cruises (see Fig. 1).

Accepte

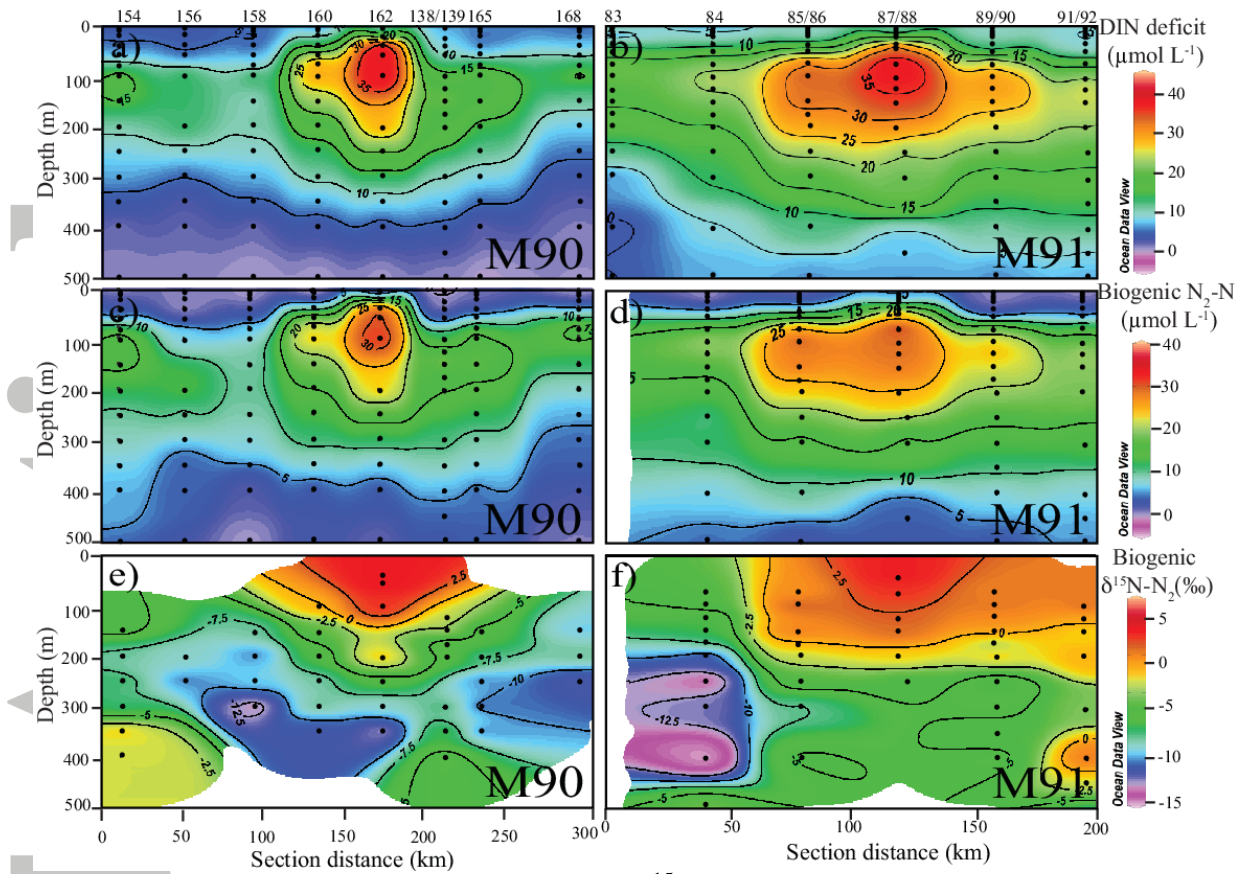


Figure 6. N_{def} (a, b), biogenic $\text{N}_2\text{-N}$ (c, d) and $\delta^{15}\text{N-N}_2$ biogenic (e, f) for transects made during the M90 (a, c, e) and M91 (b, d, f) cruises (see Fig. 1). For panels e and f, only samples with $[\text{O}_2] < 10 \mu\text{mol L}^{-1}$ and biogenic $\text{N}_2\text{-N} \geq 4 \mu\text{mol L}^{-1}$ (equivalent to the size of the propagated analytical error on our measurements) are shown.

Accepted

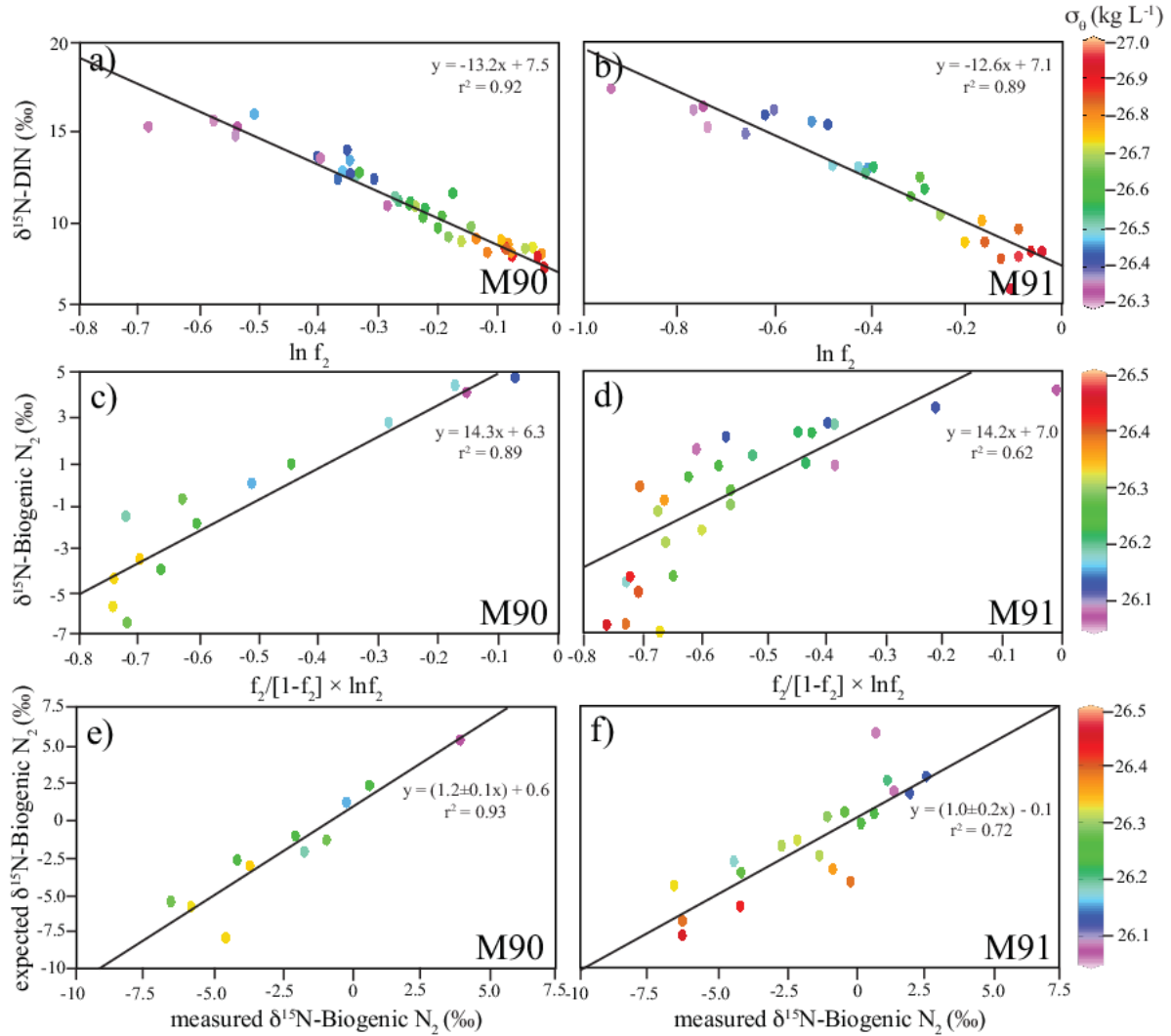


Figure 7. $\delta^{15}\text{N-DIN}$ versus $\ln f_{2-\text{bn}2}$ where $f_{2-\text{bn}2}$ = fraction of remaining NO_3^- and NO_2^- calculated using $[\text{N}_2]_{\text{biogenic}}$ (eq. 16; a and b) (σ_θ range: >26.3), $\delta^{15}\text{N-N}_2$ biogenic versus $f_{2-\text{bn}2} \times \ln f_{2-\text{bn}2}$ [1- $f_{2-\text{bn}2}$] (c and d) (σ_θ range: 26.0-26.5) and $\delta^{15}\text{N-N}_2$ biogenic exp (see eq. 8) versus measured $\delta^{15}\text{N-N}_2$ biogenic (e and f) for transects M90 (a, c, e) and M91 (b, d, f) used to calculate ϵ (ϵ = slopes) for a closed system. Only samples with $[\text{O}_2] < 10 \mu\text{mol L}^{-1}$ were considered. In a) and b), only samples >100 m depth were considered. In c) and d), only samples with biogenic $\text{N}_2 \geq 7.5 \mu\text{mol L}^{-1}$ were considered. Table 1 summarizes all ϵ calculated assuming closed and open systems for different σ_θ ranges for these transects.

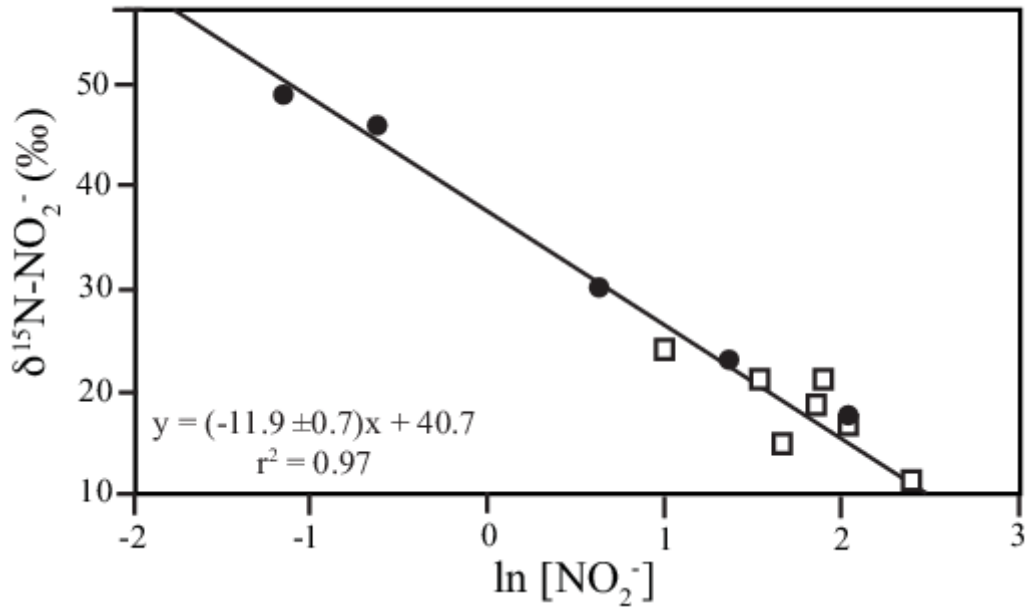


Figure 8. $\delta^{15}\text{N-NO}_2^-$ versus $[\text{NO}_2^-]$ used to calculate $^{15}\epsilon_{\text{NIR}}$ (ϵ = slope) for a closed system for the M90 (black circles) and M91 (white squares) transects. Only samples with $[\text{O}_2] < 10 \mu\text{mol L}^{-1}$ and $[\text{NO}_3^-] < 2 \mu\text{mol L}^{-1}$ were considered.

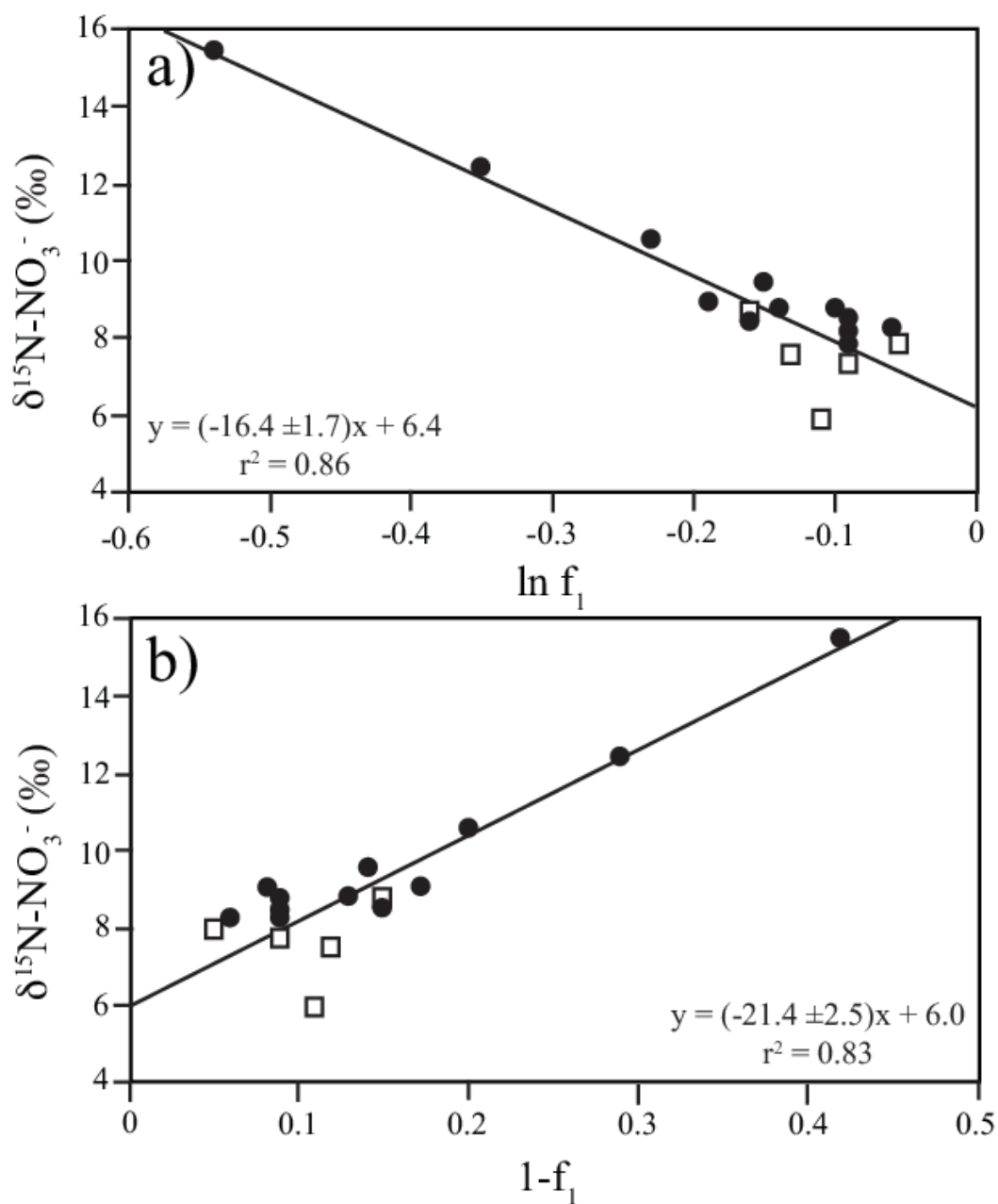


Figure 9. $\delta^{15}\text{N-NO}_3^-$ versus $\ln f_{1-\text{bN}_2}$ (eq. 15, closed system) (a), and $\delta^{15}\text{N-NO}_3^-$ versus $1-f_{1-\text{bN}_2}$ (open system) (b) used to calculate $^{15}\epsilon_{\text{NAR}}$ (ϵ = slopes) for the M90 (black circles) and M91 (white squares) transects. Only samples with $[\text{O}_2] < 10 \mu\text{mol L}^{-1}$, $[\text{NO}_2^-] < 0.05 \mu\text{mol L}^{-1}$, $> 100 \text{ m}$ depth and $\sigma_\theta > 26.3$ were considered.

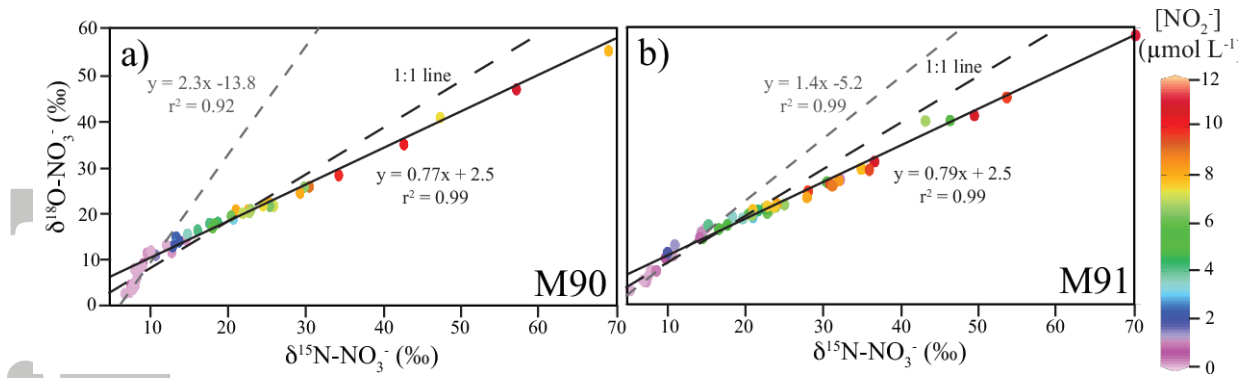


Figure 10. $\delta^{18}\text{O-NO}_3^-$ versus $\delta^{15}\text{N-NO}_3^-$ for transects M90 and M91. Linear regressions are shown for $[\text{O}_2] < 10 \mu\text{mol L}^{-1}$ (a, b). Note the different slopes where dashed grey and continuous lines represent all samples with $[\text{NO}_2^-] < 0.05 \mu\text{mol L}^{-1}$ and $\geq 0.05 \mu\text{mol L}^{-1}$, respectively. The 1:1 line expected during pure assimilatory or dissimilatory NO_3^- reduction is shown (long-dashed black line).

Accepted Article

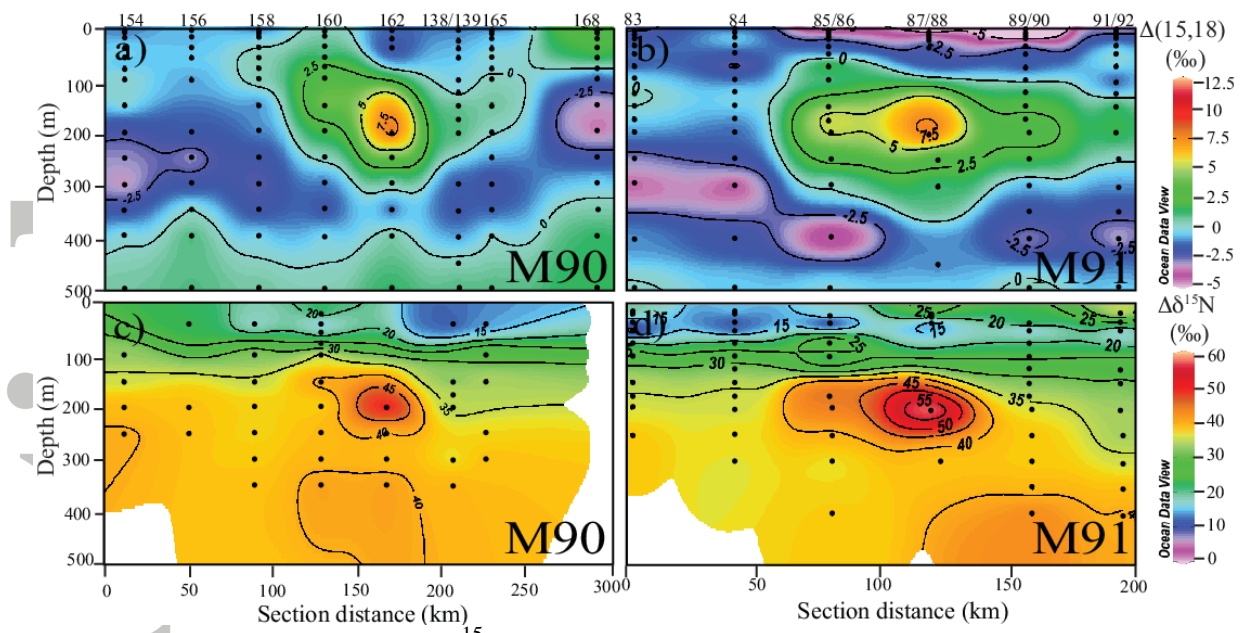


Figure 11. $\Delta(15,18)$ (a, b) and $\Delta\delta^{15}\text{N}$ (c, d) for transects M90 (a, c) and M91 (b, d) (0-500 m depth).

Accepted Article